Submitted to *Inorganic Chemistry*

REVISED VERSION. Manuscript ID ic-2020-027167

(1,2-azole)bis(bipyridyl)ruthenium(II) complexes: electrochemistry, luminescent properties, and electro- and photocatalysts for CO_2 reduction

Elena Cuéllar, Laura Pastor, Gabriel García-Herbosa, John Nganga, Alfredo M. Angeles-Boza, Alberto Diez-Varga, Tomás Torroba, Jose M. Martín-Alvarez, Daniel Miguel, and Fernando Villafañe*

ABSTRACT

New *cis*-(1,2-azole)(aquo)bis(2,2'-bipyridyl)ruthenium(II) [1,2-azole (az*H) = pzH (pyrazole), dmpzH (3,5-dimethylpyrazole), indzH (indazole)] complexes are synthesized via chlorido abstraction from *cis*-[Ru(bipy)$_2$Cl(az*H)]OTf. The latter are obtained from *cis*-[Ru(bipy)$_2$Cl$_2$], after subsequent coordination of the 1,2-azole. All the compounds are characterized by ^{1}H, ^{13}C, ^{15}N NMR and by IR. Two chlorido complexes (pzH and indzH) and two aquo complexes (indzH and dmpzH) are also characterized by X-Ray diffraction. Photophysical and electrochemical studies have been carried out on all the complexes. The photophysical data support the phosphorescence of the complexes. The electrochemical behavior in Ar atmosphere of all the complexes indicates that the oxidation processes assigned to Ru(II) → Ru(III) occur at higher potentials in the aquo complexes. The reduction processes under Ar leads to several waves, indicating that the complexes undergo successive electron transfer reductions which are centered in the bipy ligands. The first electron reduction is reversible. The electrochemical behavior in CO_2 media is consistent with CO_2 electrocatalyzed reduction, where the values of

the catalytic activity [$i_{cat}(CO_2)/i_p(Ar)$] ranged from 2.9 to 10.8. Controlled potential electrolysis for the chlorido and aquo complexes affords CO and formic acid, with the latter as the major product after two hours. All the electrochemical data are compatible with a mechanism where reductive deprotonation of the 1,2-azole ligand present in the five-coordinate complex [$Ru^0(bipy)_2(az^*H)$] would afford the active species, able to initiate the catalytic cycle by coordinating a CO_2 molecule to form the η^1-CO_2 adduct (**D**) which starts the reduction process. Photocatalytic experiments in MeCN with $[Ru(bipy)_3]Cl_2$ as photosensitizer and TEOA as the electron donor, irradiating with >300 nm light for 24 h led to CO and HCOOH as the main reduction products, achieving a combined turnover number ($TON_{CO+\ HCOO^-}$) as high as 107 for **2c** after 24 h of irradiation.

INTRODUCTION

Two of the most important global problems, *i.e.* the need for renewable energy sources and the rising levels of atmospheric CO_2, might be solved by accessing efficient and selective catalytic reduction of CO_2. Different molecular catalysts have been investigated over the past years, generating an extensive catalog of metal complexes with electrochemical and/or photochemical activity for CO_2 reduction.[1–8] The electrochemical CO_2 reduction catalyzed by *cis*-$[Ru(bipy)_2(CO)_2]^{2+}$ and *cis*-$[Ru(bipy)_2(CO)Cl]^+$ (bipy = 2,2'-bipyridine) was one of the first systems reported, back in 1987.[9] Since then, a plethora of Ru(II) catalysts have been described in the context of CO_2 catalytic reduction.

The most extensively used system in this field is *cis*-$[Ru(bipy)_2(CO)L]^{n+}$ (L = H, CO_2, C(O)OH, or CO; and n = 1, 2)[10] (**A** in chart 1). These catalysts were first introduced by Tanaka et al.[9,11–13] and were then developed also by other research groups, such as those of Meyer,[14–16] Lehn,[17,18] Fujita,[19] and Ishida.[20] These complexes are electrochemically active and readily react with carbon dioxide to form formic acid and/or carbon monoxide.

Tanaka's group[21] broadened lately the variety of compounds to those of the type $[Ru(tpy^*)(bipy^*)L]^{n+}$ (tpy* = 2,2':6',2''- terpyridine or substituted derivatives; bipy* = bipy or substituted derivatives; L = CO, MeCN, Cl; n = 1, 2) (**C** in chart 1). These catalysts were further investigated by Meyer,[22,23] Fujita,[24] Ott,[25–27] and Angeles-Boza.[28] Related complexes where one

of the coordinating atoms in the bidentate ligand is not a nitrogen atom have been developed by Masaoka[29,30] and Miller[31] (**D** in chart 1, where L = carbene or phosphine).

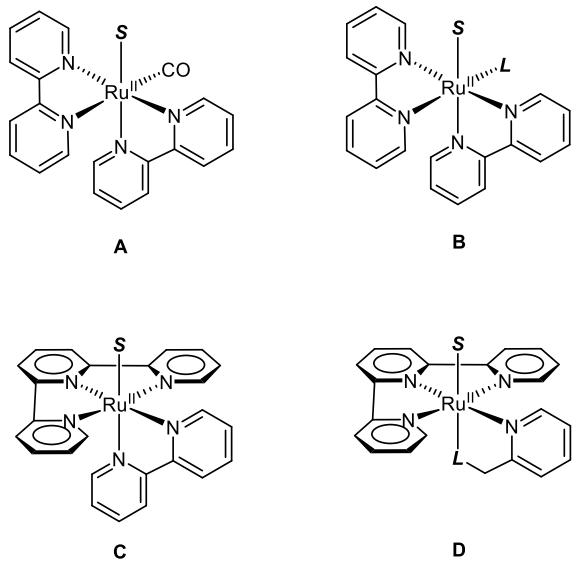

Chart 1. Ru(II) complexes studied as catalysts for CO_2 reduction: based on "*cis*-$Ru^{II}(bipy)_2$" fragments (**A** and **B**, above), and based on Ru^{II}(tpy)(bipy) (**C** and **D**, below) (**L** = Ligand, ***S*** = solvent or labile ligand).

The system by far less explored results from the coordination of a N-donor monodentate ligand into the "*cis*-$Ru(bipy)_2$" fragment, to give complexes of the type *cis*-$[Ru(bipy)_2LS]^{n+}$, (L = N-donor monodentate ligand, S = solvent or labile ligand; n = 1, 2, **B** in chart 1). This strategy would generate complexes like those containing the "Ru^{II}(bipy)(tpy)" moiety, but by easier and more straightforward synthetic procedures. Surprisingly, we have been able to find only one precedent in the literature of complexes **B** in Chart 1, described by J. Chen, who described complexes of the type *cis*-$[Ru(bipy)_2LX]^{+}$, (X = H, formate, dithioformate) and *cis*-$[Ru(bipy)_2L(NCMe)]^{2+}$, where L is a monodentate phosphine.[32]

This work reports a further contribution to this scarcely explored option, where the chosen ligand L in **B** is a 1,2-azole ligand. One of the main aspects of interest of these ligands is the presence of an acidic N-bound hydrogen. The role of acidic hydrogens in the "*cis*-$Ru^{II}(bipy)_2$" moiety has been widely explored,[33,34] and some recent studies describe the role of pH sensitive ligands,[35–38] the complexes behaviour in anion recognition,[39–43] or their DNA binding properties,[44,45] to name but a few. However, there are very scarce reports on complexes containing the bis(bipyridyl)ruthenium(II) fragment with 1,2-azole ligands. The

landmark report of T. J. Meyer's group in 1979 on cis[Ru(bipy)$_2$(pzH)$_2$]$^{2+}$ complexes and their deprotonated derivatives,[46] has been recently revisited by Hirahara et al, who has reported the role of the intramolecular hydrogen bonding in the monocationic deprotonated complex on the photosubstitution reactions.[47] The acid-base properties of [Ru(bipy)$_2$Cl(pzH)]$^+$, and the photoreactivity and biological studies of [Ru(bipy)$_2$Cl(pzH)]$^+$ have been also described.[48,49] Therefore, we focused our interest on complexes of the type **B** in Chart 1 where L is a 1,2-azole ligand and study their physical and chemical properties. We hypothesize that the presence of the 1,2-azole ligand will favor CO_2 activation given the ability of these ligands to hydrogen bond. In addition, the use of 1,2-azole ligands will favor future tunability of the complexes in both ground and excited states. We have shown how a systematic control of the electronic and steric properties of other metal transition complexes containing 1,2-azoles and their derivatives allows to tune properties of interest, such as their selectivity towards anions,[50] their luminescent properties,[51,52] or their activity as electrocatalysts in CO_2 reduction.[53]

Herein, we report the synthesis and a thorough characterization of new (1,2-azole)-aquo bis(bipyridyl)ruthenium(II) complexes. The complete characterization of the (1,2-azole)-chlorido precursors is also herein described. The 1,2-azole derivatives used in this work are pyrazole (pzH), indazole (indzH) and 3,5-dimethylpyrazole (dmpzH). The electrochemical behavior of the complexes is studied, including the behavior of the complexes synthesized as electrocatalysts for the reduction of CO_2. This study also includes the characterization and quantification of the products formed in the reduction of CO_2 catalyzed by these complexes (CO *vs*. formic acid). We have also studied the photophysical behavior of all the complexes obtained and their use as photocatalysts for the reduction of CO_2.

RESULTS AND DISCUSSION

Synthesis and characterization of the complexes

All the complexes investigated in this work and their synthesis are collected in Scheme 1. A panel of complexes with different substituents were synthesized in order to confirm the synthetic method, and also to study the influence of the substituents on the electrocatalytic reduction of CO_2. The mixed (1,2-azole)-chlorido complexes *cis*-[Ru(bipy)$_2$Cl(az*H)]OTf (**1**) (az* = pz, dmpz, indz, Scheme 1) and the (1,2-azole)-aquo complexes *cis*-

$[Ru(bipy)_2(H_2O)(az^*H)](OTf)_2$ (**2**) are included in Scheme 1. The pzH (**1a**) and dmpzH (**1c**) chlorido complexes had been previously reported by Jude *et al.*[48] and the indzH (**1b**) complex by Fonteles *et al.*[49], however, we herein describe a new synthetic procedure and report a thorough characterization. Complex *cis*-$[Ru(bipy)_2(indzH)_2](PF_6)_2$ (**3**) is included here for comparative purposes and was synthesized by the method described by Sullivan et al. for the similar bis(pyrazole) complex.[46]

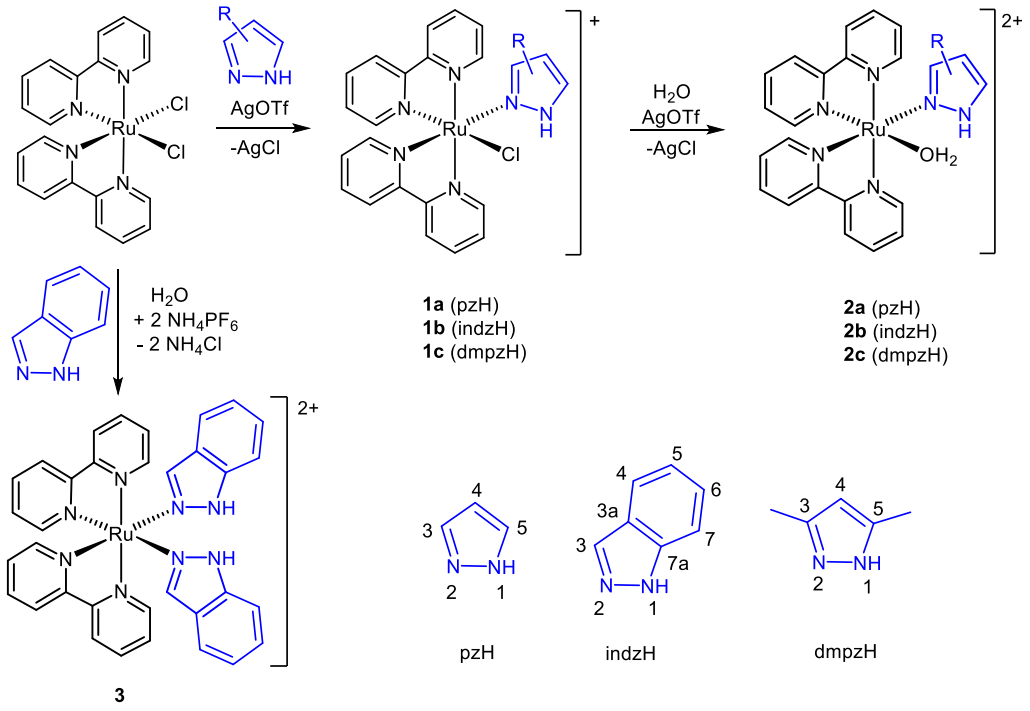

	pzH	indzH	dmpzH
cis-$[Ru(bipy)_2Cl(az^*H)]OTf$	**1a**[48]	**1b**[49]	**1c**[48]
cis-$[Ru(bipy)_2(H_2O)(az^*H)](OTf)_2$	**2a**	**2b**	**2c**
cis-$[Ru(bipy)_2(indzH)_2](PF_6)_2$		**3**	

Scheme 1. Synthesis of the complexes herein described, and 1,2-azole derivatives used, showing the numbering for NMR assignment.

Chlorido complexes **1** are obtained from *cis*-$[RuCl_2(bipy)_2]$ by abstracting one of the chlorido ligands with the stoichiometric amount of AgOTf, and subsequent addition of the 1,2-

azole. The abstraction of the second chlorido ligand in the presence of H_2O leads to the aquo complexes **2a**, **2b**, and **2c**.

The spectroscopic (^{1}H, ^{13}C and ^{15}N NMR as well as FTIR) and analytical data support the proposed geometries and are included in the Experimental section. Furthermore, complexes **1a**, **1b**, **2b** and **2c** were characterized by single-crystal X-ray diffraction studies (Figure 1). The distances and angles (CCDC 2031192-2031195) are similar to those found in other 1,2-azole ruthenium(II) complexes[54,55]. In complexes **1a** and **1b** the N-bound hydrogens of the pzH or indzH ligands are involved in hydrogen bonding with an oxygen atom of a OTf^- anion. The distances and angles determined for **1a** (H(6)···O(2) 2.269(9) Å, N(6)···O(2) 2.961(10) Å, N(6)−H(6)···O(2) 123.2(4)°) and **1b** (H(6)···O(4) 1.961(16) Å, N(6)···O(4) 2.852(17) Å, N(6)−H(6)···O(4) 143.1(5)°) may be considered as "moderate" hydrogen bonds. Moreover, in complexes **2b** and **2c** both hydrogens of the aquo ligands are involved in hydrogen bonding with an oxygen atom of an OTf^- anion, and with the oxygen atom of a solvent molecule (acetone in one cationic Ru complex in **2b**, a molecule of water in the other Ru complex in **2b** and also a water molecule in **2c**). The distances and angles detected for **2b** (H(1A)···O(16) 1.734(9) Å, O(1)···O(16) 2.657(8) Å, O(1)−H(1A)···O(16) 167.4(4)°; H(1B)···O(13) 1.828(5) Å, O(1)···O(13) 2.736(4) Å, O(1)−H(1B)···O(13) 161.8(2)°; H(2A)···O(15) 1.739(9) Å, O(2)···O(15) 2.676(8) Å, O(2)−H(2A)···O(15) 176.8(5)° and H(2B)···O(3) 1.777(7) Å, O(2)···O(3) 2.711(6) Å, O(2)−H(2B)···O(3) 173.0(3)° where O(3) and O(13) are triflate oxygens, O(15) belongs to a water molecule and O(16) to acetone) and for **2c** (H(7)··O(1) 1.757(7) Å, O(7)···O(1) 2.674(9) Å, O(7)−H(7)···O(1) 164.7(4)°) and (H(7)··O(8) 1.884(5) Å, O(7)···O(8) 2.693(6) Å, O(7)−H(7)···O(8) 142.9(4)°) may be considered also as "moderate" hydrogen bonds.

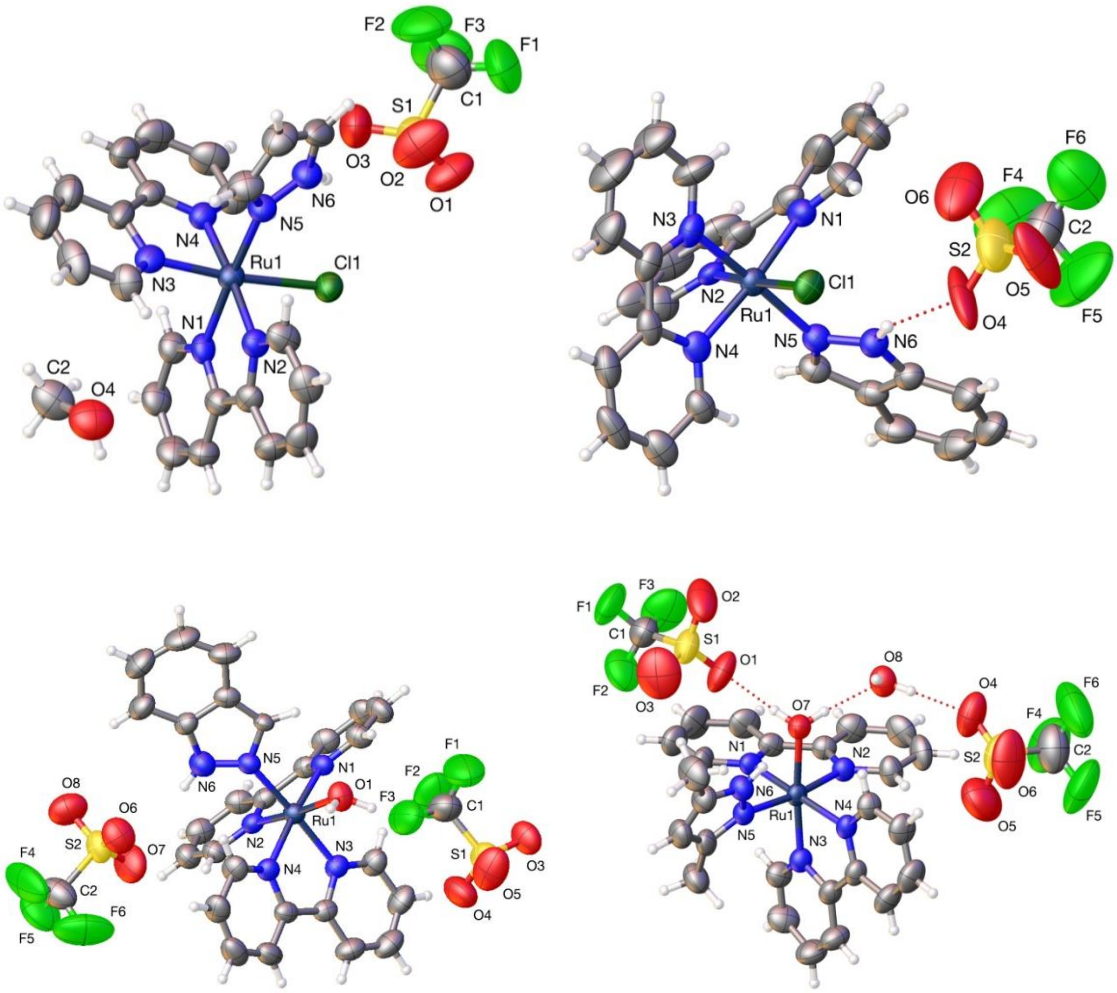

Figure 1. Perspective views of *cis*-[Ru(bipy)$_2$Cl(pzH)]OTf, **1a**, *cis*-[Ru(bipy)$_2$Cl(indzH)]OTf, **1b**, *cis*-[Ru(bipy)$_2$(H$_2$O)(indzH)](OTf)$_2$, **2b** (one of the molecules in the crystal), and *cis*-[Ru(bipy)$_2$(H$_2$O)(dmpzH)](OTf)$_2$, **2c**, showing the atom numbering. Thermal ellipsoids are drawn at 50% probability. Hydrogen bonds only shown for **1a** and **2c**, for clarity. Complete data may be found in the CIFs.

Electrochemical studies

Both the (1,2-azole)-chlorido complexes **1a**, **1b**, and **1c**, as well as the (1,2-azole)-aquo complexes **2a**, **2b**, and **2c**, showed, by cyclic voltammetry, an electrochemical behavior consistent with CO_2 activation, *i.e*. electrocatalyzed reduction (see the Supplementary Information). As a representative example, the results registered for the complex *cis*-[Ru(bipy)$_2$(H$_2$O)(IndzH)](OTf)$_2$ **2b**, are shown in Figure 2. Black (Ar) and red (CO_2) traces overlap

completely in the range −2.2V to 0.0V. Changing the atmosphere from Ar to CO_2 leads to a large enhancement of the current at potentials below −2.2V.

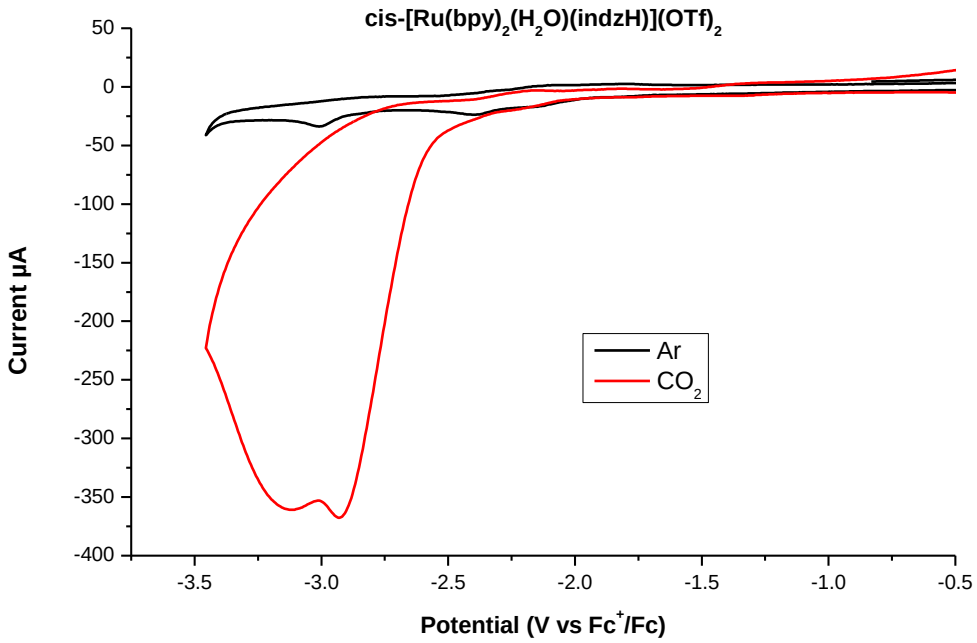

Figure 2. Cyclic voltammograms of 0.5 mM of *cis*-[Ru(bipy)$_2$(H$_2$O)(indzH)](OTf)$_2$ (**2b**) (glassy carbon working electrode dish 3.0 mm diameter, dry MeCN, 0.1 M Bu_4NPF_6) under Ar (black), and after bubbling CO_2 (red).

The cyclic voltammetry of the chlorido complexes has been previously reported, although the pyrazole and dimethylpyrazole complexes were referenced to SCE,[48] whereas the indazole complex was referenced to the AgCl/Ag electrode.[49] For this reason we have studied again the electrochemistry of all the complexes in order to reference them to the redox pair ferrocenium/ferrocene, following the IUPAC recommendations (Table 1).[56] In order to understand the exact role of the 1,2-azole ligands in the electrocatalyzed reduction process, the electrochemistry of complexes containing two 1,2-azoles, that is, *cis*-[Ru(bipy)$_2$(indzH)$_2$](PF$_6$)$_2$ (**3**), and none, *cis*-[Ru(bipy)$_2$(NCMe)$_2$](PF$_6$)$_2$ (**4**) was also studied. The synthesis and electrochemistry under N_2 of the latter has been already described.[57]

None of these previous electrochemical studies carried out on the (1,2-azole)-chlorido complexes **1** or on the bis(acetonitrile) complex **4** described their behavior in CO_2 atmosphere.

The ratio $\frac{i_{cat}(CO_2)}{i_p(Ar)}$ (Table 1) allows to compare the catalytic activity of the complexes, and the values obtained for the 1.2-azole complexes range from 2.9 to 10.8 (2.1 for the bis(acetonitrile) complex **4**). A silver wire was used in the first scan as pseudo-reference electrode, and then in the following scans the AgCl/Ag (3M NaCl) reference electrode was used. Ferrocene was added as internal calibrant always in the last experimental measurement.

Table 1. Electrochemical data obtained by cyclic voltammetry in this study and referenced to the redox system ferrocenium/ferrocene.[a]

Complex		Observed E_{pk}^{ox} and E_{pk}^{red} values.[b]					i_p(Ar)[c]	$i_{cat}(CO_2)$[c]	Ratio[d] $\frac{i_{cat}(CO_2)}{i_p(Ar)}$
		Anodic scan	Cathodic scan						
Chlorido complexes	**1a**	0.62[e]	−2.05[e]	−2.29[e]	−2.90[e]		−48	−223	4.6
	1b	0.33[e]	−2.00[e]	−2.23[e]	−2.87[e]		−47	−138	2.9
	1c	0.33[e]	−1.97[e]	−2.19[e]	−2.89[e]		−42	−132	2.9
Aquo complexes	**2a**	0.52[e]	−2.04[e]	−2.37[e]	−2.99[e]		−37	−297	8.0
	2b	0.54[e]	−2.04[e]	−2.30[e]	−2.93[e]		−34	−368	10.8
	2c	0.58[e]	−2.18[e]	−2.38[e]	−3.02[e]		−29	−188	6.5
	3	0.73[e]	−2.08[e]	−2.32[e]	−2.92	−3.00	−36	−179	5.0
	4	1.06[e]	−1.76[e]	−1.95[e]	−2.60		−62	−130	2.1

[a] The reduction potential mean value observed for Ferrocenium/Ferrocene (Fc^+/Fc) used as internal calibrant under the employed experimental conditions was E^0 = 0.443 ± 0.005 V *vs.* the AgCl/Ag (3M NaCl) electrode.

[b] Anodic or cathodic scan peaks observed under Ar unless stated otherwise.

[c] Maximum registered cathodic current (μA) under Ar, i_p(Ar), or under CO_2, $i_{cat}(CO_2)$.

[d] Ratio between the Faradaic currents observed under Ar, i_p(Ar), and under CO_2, $i_{cat}(CO_2)$.

[e] Waves where both peaks i_{ox} and i_{red} were observed. Value of $E_{1/2}$ is given in those cases.

For comparative and organizational purposes, in this section we discuss firstly the electrochemical behavior of the (1,2-azole)-chlorido complexes **1**, followed by the discussion of the (1,2-azole)-aquo complexes **2**, and finally that of *cis*-$[Ru(bipy)_2L_2]^{2+}$ [L = indzH (**3**) or NCMe

(**4**)]. For each complex, the electrochemistry under Ar atmosphere is discussed previously to the behavior under CO_2 atmosphere.

*Electrochemical behavior of complexes **1***

One reversible wave at 0.62V is detected for **1a** under GC/acetonitrile (Figure S1) whereas **1b** and **1c** display reversible waves at 0.33 V (Figures S3 and S7) (Table 1). These reversible oxidations are assigned to the Ru^{II}/Ru^{III} oxidation, and occur at higher potentials than the Ru^{II}/Ru^{III} oxidation of *cis*-$[Ru(bipy)_2Cl_2]$ (−0.06 *vs* Fc^+/Fc).[58,59] This is to be expected after the substitution of the anionic, electron donating chlorido ligand by the neutral, π-accepting 1,2-azole ligand, and the subsequent electrostatic effect of changing from neutral to cationic complexes. However, explaining the difference of potential (ca. 0.3 V) between the pzH complex **1a** *vs*. the indzH and dmpzH complexes **1b** and **1c** might be related to the fact that 1,2-azoles are deprotonable ligands. In this case the oxidation of Ru(II) might involve PCET (proton coupled electron transfer) processes with concomitant potential shifts depending on the coordinated ligand.[60,61]

Scanning the chlorido complexes **1** to negative potentials under Ar (Table 1, Figures S2, S4, S6 and S8), leads to several waves, indicating that the complexes undergo successive electron transfer reductions. This electrochemical behaviour is similar to that shown by other bis(bipyridine)ruthenium(II) complexes, and has been previously attributed to reduction processes centred at the bipyridine ligands.[49,59,62–64] However, all the complexes herein reported show a slight decrease (*ca*. 0.2-0.3 V) respect to the reduction potentials of previously reported Ru(II) complexes able to electrocatalyze CO_2 reduction.[9–31] This slight decrease is to be expected considering the fact that most of the previously reported electrocatalysts Ru(II) complexes contain CO ligand(s), which is more π-acceptor, what facilitates reduction. In order to check the reversibility of these reductions, cyclic voltammograms at different rates were performed for **1b** (Figure S5). The experiment clearly indicates that the first reduction is reversible (the 2nd and 3rd reductions in **1b** seem to overlap: compare Figures S4 and S5).

An intense enhancement of the cathodic current is observed when the same scan is repeated under CO_2 atmosphere. For **1a** (Figure S2), the maximum cathodic current under CO_2 is found at −3.00 V (*vs* Fc^+/Fc). At this potential, the ratio of the cathodic currents is

$\frac{i_{cat}(CO_2)}{i_p(Ar)} = 4.6$. For **1b** and **1c** (Figures S6 and S8 respectively), the maximum cathodic current under CO_2 were found at −2.73V and −2.94V *(vs* Fc^+/Fc) respectively. At these potentials, the ratio of the cathodic currents is $\frac{i_{cat}(CO_2)}{i_p(Ar)} = 2.9$ in both cases. The different shapes of the waves associated to electrocatalytic reduction of CO_2 come from the competition at the electrode surface between CO_2 consumption (related to the rate-determinant step of the catalytic cycle) and the arrival of new substrate by diffusion.[4]

*Electrochemical behavior of complexes **2***

At positive potentials, the cyclic voltammograms of **2a** (Figure S9), **2b** (Figure S11) and **2c** (Figure S16) show reversible waves at 0.52V, 0.54V and 0.58V *(vs* Fc^+/Fc) respectively, assigned to the Ru^{II}/Ru^{III} oxidation. These oxidation potentials are higher than those of the respective chlorido complexes, as expected after the substitution of the anionic, electron donating chlorido ligand by the neutral, σ-donating aquo ligand. Weak irreversible oxidations at slightly higher potentials are detected for some of these complexes (more clearly for **2c**, see Figure S16). The presence of an aquo ligand and the high charge of the complexes after the Ru^{II}/Ru^{III} oxidation might facilitate the deprotonation of the aquo ligand. However, no further experiments were made to identify the species responsible for these weak waves, since these processes occur during oxidation, whereas their catalytic activity is related to the reduction processes. Complexes **1**, **2**, and **3** are stable in MeCN solutions when no potential is applied, as confirmed by ^{1}H NMR spectra in CD_3CN even after 24 h at r.t.

Scanning to negative potentials under Ar (Figures S10, S12, S15, and S17) allows to observe several waves, as the result of successive electron transfer reductions. Cyclic voltammograms at different rates were performed for **2b** (Figures S13 and S14) in order to check the reversibility of these reductions. As for **1b**, the results indicate again that the first reduction is reversible. Again, intense enhancements of the cathodic currents are detected when the same scan is carried out under CO_2 atmosphere. The maximum cathodic current under CO_2 is found at −3.20V, −2.92V and −3.13V *(vs* Fc^+/Fc) respectively for **2a**, **2b**, and **2c**. At this potential, the ratio of the cathodic currents $\frac{i_{cat}(CO_2)}{i_p(Ar)}$ is 8.0 for **2a,** 10.8 for **2b** and 6.5 for **2c**.

*Electrochemical behavior of complexes **3** and **4***

As indicated above, the dicationic complex *cis*-[Ru(bipy)$_2$(indzH)$_2$](PF$_6$)$_2$ (**3**) was synthesized and studied in order to determine the exact role of the 1,2-azole ligands in this electrocatalyzed reduction process. The synthesis and electrochemistry of the similar bis(pyrazole) complex has been already described.[46] Compound **3** shows a reversible wave at 0.73V (*vs* Fc^+/Fc) corresponding with the Ru(II)/Ru(III) oxidation (Table 1, Figure S13). As reported for the similar bis(pyrazole) complex,[46] a less intensive wave at 0.38V (*vs* Fc^+/Fc) is also observed, which is assigned to the oxidation of the deprotonated monocationic *cis*-[Ru(bipy)$_2$(indz)(indzH)]PF$_6$ complex, formed in situ.[65] As for complexes **1** and **2**, scanning to negative potentials under Ar (Table 1, Figures S19, and S22) leads to several waves, indicating that **3** undergoes successive electron transfer reductions, attributed to reduction processes centered at the bipyridine ligands, as indicated above. Again, the cyclic voltammograms at different rates performed for **3** (Figure S20) support that the first reduction is reversible. Finally, the electrochemical behavior in CO_2 media (Table 1, Figure S21) is also consistent with CO_2 electrocatalyzed reduction, where the value of the catalytic activity $\frac{i_{cat(CO_2)}}{i_p(Ar)}$ is 5, that is, a similar value to those obtained for the complexes **1** and **2**, which contain only one 1,2-azole ligand.

The electrochemical behavior in CO_2 of the bis(acetonitrile) complex **4** is herein described, since it has not been previously reported. It is indicative of a very weak CO_2 electrocatalyzed reduction (Table 1, Figure S22), with a value of the catalytic activity $\frac{i_{cat(CO_2)}}{i_p(Ar)}$ of 2.1, that is, clearly below those obtained for the complexes **1**, **2**, and **3**, which contain 1,2-azole ligands.

Electrocatalysis voltammetry

The mechanism for the electrocatalytic reduction of CO_2 with complexes containing the "cis-Ru^{II}(bipy)$_2$" moiety is well established,[1,4] and starts with a one-electron reduction followed immediately by a second one-electron reductive dehalogenation, which affords a five-coordinate species of the type [Ru^0(bipy)$_2$L]. This neutral complex is the active species which initiates the catalytic cycle by coordinating a CO_2 molecule to form the η^1-CO_2 adduct required to start the reduction process. In our case, the first reduction is always reversible, as indicated above (Figures S5 for **1b**, S13 and S14 for **2b**, and S20 for **3**), and the onset potential of the CO_2 reduction always occurs after the second or with the third electron reduction process (see

Figure 2, as well as Figures S2, S6, S8, S10, S15, S17, and S21). We have found a precedent in the literature where this situation occurs,[24] and it is related to the presence of acidic OH groups near the Ru(II) centre. In that case, reductions of the complexes were irreversible due to reductive deprotonation of the ligands. As the 1,2-azole ligands present in our complexes contain also an acidic proton, a similar process might be herein proposed, where the third reduction observed in the cyclic voltammograms occurs with a reductive deprotonation.

A second effect observed is the higher catalytic activity of the aquo complexes compared to that of the chlorido complexes. This is to be expected, because of the higher lability of the hard aquo ligand in comparison with the softer chlorido ligand when coordinated to a soft metallic centre, such as Ru(II). After the reduction observed in the voltammograms, this effect should be even more pronounced, since reduction occurs with further softening of the metallic centre.

A third important feature is the peak of the enhanced current at reduction potentials reached by the complexes, which is ca. −3 V for all them, except for **1b** and **1c**, where the plateau is reached at −2.7 V or −2.6 V (see Figures S2, S6, S8, S10, S15, S17, and S21), thus improving the overpotential η_{cat} parameter by 0.3 and 0.4 volts respectively. This is also observed in Table 2, and it is supported by the experiment described in the next paragraph. Finally, the presence of the 1,2-azole ligands in the electrocatalytic reduction of CO_2 seems to be a determining factor, possibly helping to stabilize some of the intermediates active in the catalytic cycle. It should be also pointed out that the onset potential of the CO_2 reduction in the bis(acetonitrile) complex **4** occurs after the third electron reduction process (see Figure S22), what suggest that the lower catalytic activity in this complex may occur by a different mechanism.

Controlled potential electrolysis

To further evaluate the catalytic activity of the ruthenium complexes described in this work, we performed controlled potential electrolysis (CPE) studies. CPE was carried out in CH_3CN using a three-electrode set-up with a glassy carbon working electrode and at −2.7 V vs the Fc^+/Fc couple. The gaseous products, H_2 and CO, were then analyzed by sampling the headspace of the electrolysis cell using gas chromatography. The determination of formic acid was accomplished using ^1H NMR spectroscopy.[66] The results, compiled in Table 2, show that the catalysts are selective towards the reduction of CO_2 over that of protons. Two products are

formed from CO_2, formic acid and CO, the former being produced at higher yields than the latter. The formation of formic acid may be due to the presence of adventitious water present in the experiment, as reported by other groups.[4] No signals of free 1,2-azole were detected in the ^{1}H NMR spectra recorded after the CPE experiments, what is an indication of the high stability of the complexes during the catalytic process. Just as observed in the cyclic voltammetry experiments, the aquo complexes are more active and produced *c.a.* 20% more product than their chloride counterparts.

Table 2. Faradaic efficiencies and turnover numbers (TON) for all complexes in acetonitrile after CPE experiments with a reticulated vitreous carbon working electrode held at –2.7 V for 2 hours.

Catalyst	FE at –2.7 V[a]			TON		TOF[b] (h^{-1})	
	H_2	CO	HCOOH	CO	HCOOH	CO	HCOOH
1a	<1%	31%	44%	2.6	5	1.3	2.5
1b	<1%	34%	47%	3	5.1	1.5	2.5
1c	<1%	30%	44%	2.9	5	1.5	2.5
2a	<1%	32%	54%	3.4	6.1	1.7	3.1
2b	<1%	35%	52%	3.8	5.9	1.9	2.9
2c	<1%	29%	48%	3.5	5.1	1.7	2.5
3	<1%	30%	49%	2.8	5.1	1.4	2.5
4	<1%	26%	39%	2.3	4.2	1.2	2.1

[a]Potential V vs Fc/Fc^+. [b]Determined from CPE.

With all these data in mind, a mechanism may be proposed in order to explain the electrochemical catalysis, displayed in Scheme 2. The first reduction is assumed to occur at the bipyridine ligands and is reversible giving **A**. The second reduction should occur with elimination of the weaker ligand (chlorido in **1**, aquo in **2**, indzH in **3**) affording the five-coordinate complex $[Ru^0(bipy)_2(1,2\text{-azole})]$, **B**. Reductive deprotonation of the 1,2-azole ligand would afford **C**, which should be the active species, initiating the catalytic cycle by coordinating a CO_2 molecule to form the η^1-CO_2 adduct (**D**) which starts the reduction process. According to the well established mechanism for the electrocatalytic reduction of CO_2 with complexes containing the "*cis*-$Ru^{II}(bipy)_2$" moiety, the protonation (in our case probably by the presence of traces of water) with removal of a water molecule would give **E**. The cycle would finish with decarbonilation of **E** coupled with a two-electron reduction, leading again to the initial active species **C**. The formation of formic acid may be explained considering the protonation of **C** to five the hydrido complex **F**, which would insert CO_2 to give the species with a formato ligand **G**. The protonation of the latter would liberate formic acid, with concomitant two electron

reduction leading again to **C**. The formation of formic acid through an hydrido intermediate has been previously supported.[14,28,67] Therefore, the observed formation of CO or formic acid depends on which path takes place from of the η^1-CO_2 adduct **D**.

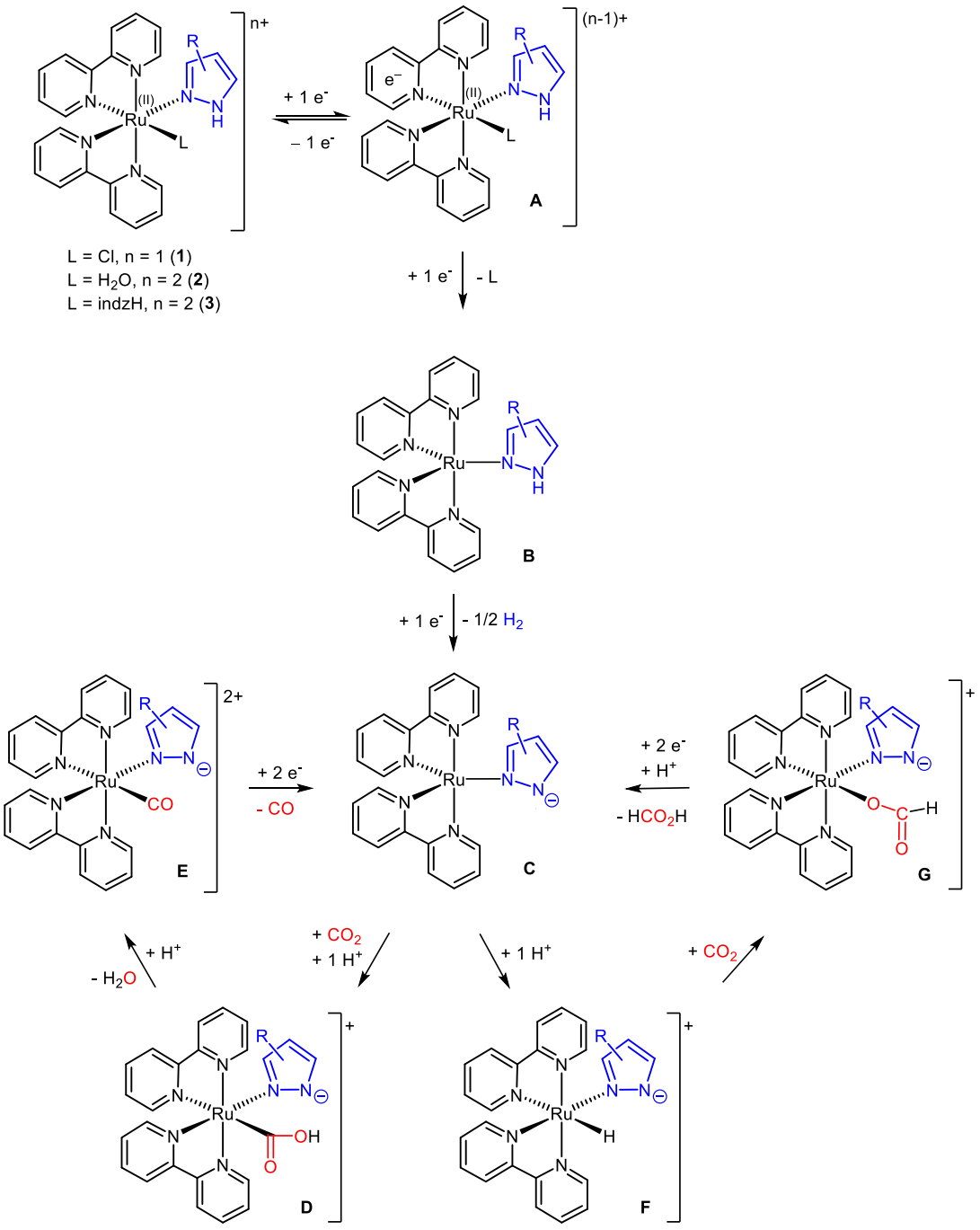

Scheme 2. Mechanism proposed in order to explain the electrochemical catalysis of complexes **1**, **2**, and **3**.

Photophysical studies.

The absorption and emission spectral data for complexes **1** and **2** are summarized in Table 3 and Table 4. Complexes **3** and **4** did not show any luminescent behavior. The absorption spectral data of the pzH (**1a**) and dmpzH (**1c**) chlorido complexes had been previously reported by Jude *et al.*,[48] and the indzH (**1b**) complex was characterized by Fonteles *et al.*[49] However, we have measured again all of them under the same conditions in order to compare the results with those of the (1,2-azole)-aquo complexes **2**. The absorption and emission spectra (those of **2a** are shown in Figure 3), as well as the wavelengths maxima detected in different deaerated solvents at 298 K are collected in the supporting information (Figure S23). The spectra show absorption profiles similar to previously reported complexes of this type.[46,59] All the complexes display intense absorption bands in the 250-300 nm region which may be attributed to π(L)→π*(L) IL, and lower energy broad bands above 300 nm, corresponding to dπ(Ru)→π*(L) MLCT. The low energy band of all the complexes are blue shifted when the chlorido ligand is substituted by the aquo ligand. These blue shifts are originated by electronic effects induced by the substitution of the anionic, electron donating chlorido ligand by the neutral, σ-donating aquo ligand.

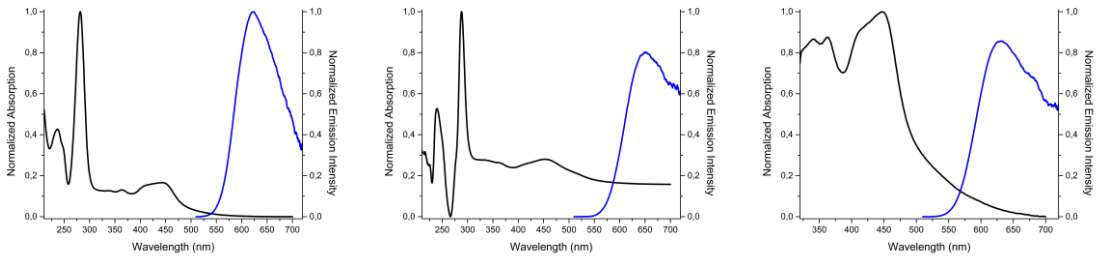

Figure 3. Normalized UV/vis absorption (black) and emission (blue, λ_{ex} = 420 nm) spectra at 298 K, in optically dilute solutions of **2a** in MeCN (left), THF (center), and acetone (right).

The emission spectra show one unstructured broad band, which are solvent-dependent (around 20 nm shifts for all the complexes). The intensities in the emission spectra show a dramatic increase in deaerated solutions compared to those prepared without exclusion of air, with no variation in the emission maxima (Figure S24). These results, along with luminescent emission lifetimes (see below), are characteristic features of ^{3}MLCT phosphorescent emissions.[68,69]

Table 3. Absorption and emission data of complexes in MeCN.

Comp	Absorption	Emission
	λ nm (ε x 10^{-3} $M^{-1}cm^{-1}$)	λ_{em} nm [λ_{excit} = 420 nm]
1a	237 (19.9), 287 (49.5), 341 (7.3), 477 (7.3)	625
1b	236 (24.1), 287 (54.9), 338 (8.1), 476 (8.3)	646
1c	236 (23.5), 287 (55.8), 341 (8.6), 473 (8.5)	640
2a	237 (18.3), 282 (43.1), 339 (5.4), 364 (5.5), 444 (7.1)	624
2b	232 (21.8), 281 (48.9), 333 (5.9), 373 (8.1), 411 (9.2), 429 (9.0)	621
2c	236 (19.4), 283 (43.9), 342 (6.5), 358 (6.4), 455 (6.9)	638

Table 4. Emission data of complexes in different solvents.

Comp		Emission				
	Solvent	**Ø ×10^{-2}**	**τ / ns**	**χ^2**	**$k_r/10^4$ s^{-1}**	**$k_{nr}/10^4$ s^{-1}**
1a	THF	1.41	46.1	1.01	30.6	2138.6
1b	MeCN	0.15	42.1	1.30	3.6	2371.7
1c	MeCN	0.92	178.5	1.18	5.2	555.1
2a	THF	2.23	37.3	1.08	59.8	2621.2
2b	THF	1.33	64.9	1.05	20.5	1520.3
2c	MeCN	1.01	144.9	1.11	7.0	683.2

As the solvent does not affect the quantum yields and the luminescent emission lifetimes, they have been measured in different solvents depending on their solubility (Table 4). Both are similar to those reported for other bis(bipyridine)ruthenium(II) complexes.[63] The comparison among the quantum yields of (1,2-azole)-aquo complexes **2** with the (1,2-azole)-chlorido complexes **1** leads to significant variations, showing that complexes **2** have higher quantum yield in all the cases. A reviewer points out the higher values of the luminescent emission lifetimes for complexes **1c** and **2c** compared to the rest. Unfortunately, we are unable to find an straightforward explanation for this feature. The radiative and non-radiative rate-constants **1c** and **2c** are shorter than those for the other complexes, what is also in accordance with their lesser values of quantum yields. The data obtained for all complexes are well described by single-exponential decays, as indicated by the quality-of-fit χ2 ranged in 1.01 - 1.30, close to the ideal value of 1.

Photocatalytic experiments

The complexes herein described are both catalyst for CO_2 reduction and luminescent, therefore, we decided to explore their activity as photocatalysts. However, the results of the experiments carried out with these complexes as both the photocatalyst and photosensitizer were unsatisfactory. Therefore, we decided to explore their photocatalytic activity in the presence of $[Ru(bipy)_3]^{2+}$. The photocatalytic CO_2 reduction experiments were carried out in a CO_2 saturated CH_3CN-TEOA (5:1 v/v) solution containing a mixture of catalyst and $[Ru(bipy)_3]^{2+}$ as the photosensitizer in a glass vial with a volume of 10 mL under continuous irradiation (light intensity = 150 mW/cm^2, 25 °C, λ > 300 nm) (Table 5). To validate the photocatalytic data, various control experiments under different experimental conditions were carried out under irradiation with light. In the absence of $[Ru(bipy)_3]^{2+}$, catalyst or the sacrificial electron donor, TEOA, only trace amounts of product or none was produced, indicating that all the three components are necessary for efficient CO_2 activation. Formic acid produced was quantified using the protocol reported by Kubiak et al.[70] For all complexes, after 24 h, formic acid production was 2-3 times that of CO formation.

Recently, a similar complex, $[Ru(bipy)_2(CO)_2]^{2+}$, was shown to produce formic acid over CO under similar photocatalytic conditions using $[Ru(bipy)_3]^{2+}$ as a photosensitizer.[71] When a different photosensitizer, $[Ir(ppy)_3]$ (ppy = 2-phenylpyridine), was used the ratio of products changed to favor CO formation, regardless of whether acetonitrile or DMF was used as a solvent. All photocatalysts produced similar amounts of products, with TON for the production of formic acid ranging from 48 to 76, whereas TON for CO formation varied from 12 to 31. It is likely that more formate is produced under these reaction conditions since the presence of traces of water can act as the source of protons. ^{1}H NMR experiments show that mixing complexes **1**, **2**, or **3** in CD_3CN solution with excess TEOA does not deprotonate the 1,2-azole. However, the option that deprotonation by TEOA might occur in the reduced complexes can not be completely discarded, even though the 1,2-azole ligand would be less acidic in these conditions. Similarly to the electrocatalysis results, the aquo complexes are the best photocatalysts under these reaction conditions. It is likely that for the photocatalysts presented in this work the reaction conditions can be optimized for the production of either CO or formic acid, as demonstrated by Rodrigues *et al.*,[73] thus, we will not speculate on the influence of the ligands towards selectivity.

Table 5. Photocatalytic experiments with Ru complexes (0.1mM) in a solvent mixture of CH3CN-TEOA (5:1 v/v) with 1.6mM $[Ru(bipy)_3]Cl_2$ as photosensitizer (PS) and TEOA as the electron donor (ED). Two of the control experiments are shown in entries 7 and 8. Irradiation with >300 nm light for 24 h, light intensity = 150 mW/cm^2, 25 °C.

Entry	Catalyst	PS	CO (μmol)	CO (TON)	HCOOH (μmol)	HCOOH (TON)	H_2 (μmol)	Φ (%)	
								CO	HCOOH
1	**1a**	$[Ru(bipy)_3]^{2+}$	5.1	21	15	60	2	0.58	2.8
2	**1b**	$[Ru(bipy)_3]^{2+}$	4.4	18	16	66	4	0.68	1.8
3	**1c**	$[Ru(bipy)_3]^{2+}$	5.8	23	13	56	3	0.56	2.3
4	**2a**	$[Ru(bipy)_3]^{2+}$	7.2	28	18	68	3	0.69	3.1
5	**2b**	$[Ru(bipy)_3]^{2+}$	5.6	23	17	70	2	0.75	2.1
6	**2c**	$[Ru(bipy)_3]^{2+}$	7.6	31	19	76	3	0.85	3.5
7	**3**	$[Ru(bipy)_3]^{2+}$	4.5	18	16	66	3	0.58	3.1
8	**4**	$[Ru(bipy)_3]^{2+}$	3.2	12	11	48	2	0.68	1.3
9	**1a**	-	<1	<2	<1	<1	<1	-	-
10	**1a**[a]	$[Ru(bipy)_3]^{2+}$	-	-	-	-	-	-	-

[a]Entry 10. TEOA was not added to the mixture.

CONCLUSIONS

A family of the scarcely explored complexes of the type $[Ru^{II}(bipy)_2LX]$, (L = N-donor monodentate ligand; X = halido or labile ligand) are described (herein L is a 1,2-azole derivative and X is Cl or H_2O). Four of them have been crystallographically characterized. The complexes show phosphorescent behaviour with quantum yields comparable to that of other ruthenium(II) complexes. The complexes efficiently reduce, both electrochemically and photochemically, CO_2 into CO and formic acid. Formic acid is the major product in the reactions. A plausible mechanism for this process is herein provided, where reductive deprotonation of the 1,2-azole ligand present in the five-coordinate species $[Ru^0(bipy)_2(1,2\text{-azole})]$ would afford the active species. Among the metal complexes with electrochemical and/or photochemical activity for CO_2 reduction, this is a very viable option, as they can be easily synthesized and may allow a fine tuning of the electrochemical, luminescent and

catalytic activity simply by using different 1,2-azoles (or other ligands) or by substituting the chlorido or aquo ligand by different donors. Further studies in this direction are currently underway.

EXPERIMENTAL SECTION

General remarks. All manipulations were performed under a N_2 atmosphere following conventional Schlenk techniques. Solvents were purified according to standard procedures. *cis*-[Ru(bipy)$_2$Cl$_2$],[52] was obtained as previously described by our group. All other reagents were obtained from the usual commercial suppliers and used as received. Infrared spectra were recorded in solid in a Bruker Tensor 27 FTIR. Standard abbreviations are used to indicate intensity: w = weak, m = medium, s = strong, vs = very strong. NMR spectra were recorded on 500 MHz Agilent DD2 and 400 MHz Agilent MR instruments in the Laboratorio de Técnicas Instrumentales (LTI), University of Valladolid, using $(CD_3)_2CO$ or $(CD_3)_2SO$ as solvents at room temperature (r.t.). ^{1}H, ^{13}C NMR and ^{15}N NMR chemical shifts (δ) are reported in parts per million (ppm) and are referenced to tetramethylsilane (TMS, for ^{1}H and ^{13}C NMR) or to nitromethane (CH_3NO_2, for ^{15}N NMR), using the residual solvent peak as an internal reference. Coupling constants (*J*) are reported in Hz. Standard abbreviations are used to indicate multiplicity: s = singlet, d = doublet, ddd=doublet of doublet of doublets, dt= doublet of triplets, t = triplet, m = multiplet. The full assignment of the ^{1}H NMR spectra was supported by typical homonuclear ^{1}H-^{1}H correlations such as COSY, TOCSY and NOESY experiments and the assignment of ^{13}C{^{1}H} and ^{15}N NMR data was supported by HMBC and HSQC heteronuclear experiments (Figure 4). Elemental analyses were performed on a Thermo Fisher Scientific EA Flash 2000.

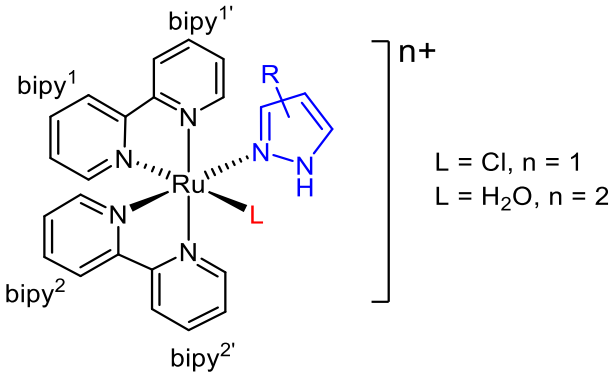

Figure 4. Numbering of bipy for NMR assignment.

***cis*-[Ru(bipy)$_2$Cl(pzH)]OTf, 1a.** This complex was prepared by a modification of the method previously described in the literature. Its synthesis and some spectroscopic data have been previously reported.[48]

AgOTf (0.256 g, 1.0 mmol) was added to a mixture of *cis*-[Ru(bipy)$_2$Cl$_2$] (0.520 g, 1.0 mmol) in MeOH (40 mL), and the mixture was stirred at r.t. for 24 h in the absence of light. The solution was filtered to remove solid AgCl. pzH (0.068 g, 1.0 mmol) was then added, and the mixture was stirred at 40°C for 24 h. The solvent was then removed in vacuo to give a red solid, which was washed with Et_2O (3 x 5 mL approximately), and dried in vacuo, yielding 0.579 g (87%). ^{1}H NMR (500 MHz, Acetone-d_6) δ: 12.78 (s, NH pzH, 1 H), 9.99 (d, *J* = 1.1 Hz, H$^{6'}$ bipy^1, 1 H), 8.72 (d, *J* = 8.1 Hz, H$^{3'}$ bipy^2, 1 H), 8.69 (d, *J* = 8.2 Hz, H$^{3'}$ bipy^1, 1 H), 8.65 (d, *J* = 8.2 Hz, H^3 bipy^1, 1 H), 8.60 (d, *J* = 8.1 Hz, H^3 bipy^2, 1 H), 8.27 (d, *J* = 5.4 Hz, H$^{6'}$ bipy^2, 1 H), 8.16 (t, *J* = 7.9 Hz, H$^{4'}$ bipy^1 and H$^{4'}$ bipy^2, 2 H), 8.06 (d, *J* = 4.4 Hz, H^6 bipy^1, 1 H), 8.03 – 7.96 (m, H^5 pzH and H^4 bipy^1, 2 H), 7.94 (td, *J* = 7.9, 1.4 Hz, H^4 bipy^2, 1 H), 7.83 (d, *J* = 5.1 Hz, H^6 bipy^2, 1 H), 7.79 (ddd, *J* = 7.4, 5.7, 1.3 Hz, H$^{5'}$ bipy^1, 1 H), 7.69 (ddd, *J* = 7.4, 5.6, 1.3 Hz, H$^{5'}$ bipy^2, 1 H), 7.39 (ddd, *J* = 7.4, 5.7, 1.4 Hz, H^5 bipy^1, 1 H), 7.31 (ddd, *J* = 7.3, 5.7, 1.3 Hz, H^5 bipy^2, 1 H), 6.66 (t, *J* = 1.8 Hz, H^3 pzH, 1 H), 6.37 (dd, *J* = 2.3 Hz, H^4 pzH, 1 H). ^{13}C NMR (126 MHz, Acetone-d_6) δ: 160.01 (1C, C^2 bipy^1), 159.02 (1C, C^2 bipy^2), 158.31 (1C, C$^{2'}$ bipy^2), 157.98 (1C, C$^{2'}$ bipy^1), 153.09 (1C, C^6 bipy^1), 153.01 (1C, C$^{6'}$ bipy^1), 152.17 (1C, C^6 bipy^2), 152.08 (1C, C$^{6'}$ bipy^2), 139.75 (1C, C^3 pzH), 136.25 (1C, C$^{4'}$ bipy^2), 136.02 (1C, C$^{4'}$ bipy^1), 135.88 (1C, C^4 bipy^2), 135.58 (1C, C^4 bipy^1), 131.58 (1C, C^5 pzH), 126.79 (1C, C^5 bipy^1), 126.60 (1C, C$^{5'}$ bipy^2), 126.37 (1C, C$^{5'}$ bipy^1), 125.94 (1C, C^5 bipy^2), 123.72 (1C, C^3 bipy^1), 123.31 (1C, C$^{3'}$ bipy^2), 123.2 (1C, C$^{3'}$ bipy^1)7, 123.00 (1C, C^3 bipy^2), 107.48 (1C, C^4 pzH). ^{15}N NMR (51 MHz, Acetone-d_6) δ: −116.80 (1N, N$^{1'}$ bipy^2), −121.20 (1N, N$^{1'}$ bipy^1), −121.66 (1N, N^2 pzH), −124.84 (1N, N^1 bipy^2), −127.13 (1N, N^1 bipy^1), −172.33 (1N, N^1 pzH)). IR (solid, cm^{-1}): 3598 w, 3529 w, 3250 m, 3108 w, 3076 w, 2288 w, 2189 w, 2165 w, 2141 w, 2113 w, 2051 w, 1981 w, 1625 w, 1602 m, 1562 w, 1520 w, 1483 w, 1463 s, 1444 s, 1419 s, 1348 w, 1257 vs, 1224 vs, 1148 vs, 1123 vs, 1055 m, 1029 vs, 968 w, 888 w, 857 w, 801 w, 761 vs, 730 vs, 659 m, 635 vs. Anal. Calcd for **1a**·CH_3CO $C_{26}H_{23}ClF_3N_6O_4RuS$: C, 44.03; H, 3.26; N, 11.85; S, 4.52. Found: C, 43.91; H, 3.05; N, 12.10; S, 4.62.

***cis*-[Ru(bipy)$_2$Cl(indzH)]OTf, 1b.** This complex was prepared by a modification of the method previously described in the literature. Its synthesis and some spectroscopic data have been previously reported.[49]

To a solution containing [Ru(bipy)$_2$Cl(OTf)] (1.0 mmol) in MeOH (40 mL), obtained as indicated for **1a**, indzH (0.118 g, 1.0 mmol) was added, and the mixture was stirred at 50°C for 24 h. Work up as for **1a** gave **1b** as a red solid. Yield 0.630 g (88%). ^{1}H NMR (500 MHz, Acetone-d_6) δ 12.83 (s, NH indzH, 1 H), 9.99 (d, J = 5.6 Hz, H$^{6'}$ bipy^1, 1 H), 8.75 – 8.63 (m, H^3 bipy^1, H$^{3'}$ bipy^1 and H$^{3'}$ bipy^2, 1 H), 8.61 (d, J = 8.2 Hz, H^3 bipy^2, 1 H), 8.41 (d, J = 5.5 Hz, H$^{6'}$ bipy^2, 1 H), 8.18 – 8.05 (m, H$^{4'}$ bipy^2, H$^{4'}$ bipy^1 and H^6 bipy^1, 3 H), 8.00 (t, J = 7.9 Hz, H^4 bipy^1, 1 H), 7.93 (t, J = 7.9 Hz, H^4 bipy^2, 1 H), 7.82 (d, J = 5.6 Hz, H^6 bipy^2, 1 H), 7.81 – 7.71 (m, H^7 indzH, H$^{5'}$ bipy^1, 1 H), 7.62 (t, H$^{5'}$ bipy^2, 1 H), 7.57 (d, J = 8.2 Hz, H^4 indzH, 1 H), 7.45 – 7.35 (m, H^3 indzH, H^6 indzH and H^5 bipy^1, 3 H), 7.32 (t, H^5 bipy^2, 1 H), 7.13 (t, J = 7.6 Hz, H^5 indzH, 1 H). ^{13}C NMR (126 MHz, Acetone-d_6) δ 159.85 (1C, C^2 bipy^1), 158.71 (1C, C^2 bipy^2), 158.16 (1C, C$^{2'}$ bipy^2), 157.91 (1C, C$^{2'}$ bipy^1), 153.10 (1C, C^6 bipy^1), 152.96 (1C, C$^{6'}$ bipy^1), 152.28 (1C, C$^{6'}$ bipy^2), 152.00 (1C, C^6 bipy^2), 140.88 (1C, C^{7a} indzH), 136.55 (1C, C$^{4'}$ bipy^1), 136.22 (1C, C$^{4'}$ bipy^2), 136.16 (1C, C^4 bipy^2), 136.01 (1C, C^3 indzH), 135.89 (1C, C^4 bipy^1), 127.60 (1C, C^6 indzH), 127.01 (1C, C^5 bipy^1), 126.69 (1C, C$^{5'}$ bipy^2), 126.46 (1C, C$^{5'}$ bipy^1), 126.03 (1C, C^5 bipy^2), 123.94 (1C, C$^{3'}$ bipy^1), 123.82 (1C, C^{3a} indzH), 123.46 (1C, C^3 bipy^1), 123.40 (1C, C$^{3'}$ bipy^2), 123.06 (1C, C^3 bipy^2), 121.73 (1C, C^5 indzH), 119.72 (1C, C^4 indzH), 110.27 (1C, C^7 indzH). ^{15}N NMR (51 MHz, Acetone-d_6) δ: −117.96 (1N, N$^{1'}$ bipy^2), −122.63 (1N, N$^{1'}$ bipy^1), −125.19 (1N, N^1 bipy^2), −128.08 (1N, N^1 bipy^1), −132.97 (1N, N^2 indzH), −195.70 (1N, N^1 indzH). IR (solid, cm^{-1}): 3496 w, 3265 w, 3108 w, 3074 w, 2973 w, 2873 w, 1739 w, 1624 w, 1603 w, 1566 w, 1508 w, 1485 m, 1462 m, 1445 m, 1421 m, 1378 w, 1354 w, 1313 w, 1257 vs, 1234 s, 1221 vs, 1145 s, 1123 m, 1112 m, 1073 w, 1029 vs, 962 w, 901 w, 875 w, 830 w, 802 w, 755 vs, 729 vs, 659 w, 634 vs. Anal. Calcd for $C_{28}H_{22}ClF_3N_6O_3RuS$: C, 46.96; H, 3.10; N, 12.74; S, 4.48. Found: C, 46.40; H, 3.07; N, 12.42; S, 4.32.

***cis*-[Ru(bipy)$_2$Cl(dmpzH)]OTf, 1c.** This complex was prepared by a modification of the method previously described in the literature. Its synthesis by conventional methods and some spectroscopic data have been previously reported.[48]

To a solution containing [Ru(bipy)$_2$Cl(OTf)] (1.0 mmol)in MeOH (40 mL), obtained as indicated for **1a**, dmpzH (0.111 g, 1.0 mmol) was added, and the mixture was stirred at 50°C for 24 h. Work up as for **1a** gave **1c** as a red solid. Yield 0.583 g (84%). ^{1}H NMR (500 MHz, Acetone-d_6) δ 12.40 (s, NH dmpzH, 1 H), 10.03 (d, J = 5.6 Hz, H$^{6'}$ bipy^1, 1 H), 8.74 (d, J = 8.2 Hz,

$H^{3'}$ bipy^2, 1 H), 8.67 (d, *J* = 9.1 Hz, $H^{3'}$ bipy^1, 1 H), 8.60 (d, *J* = 8.2 Hz, H^3 bipy^1 and H^3 bipy^2, 2 H), 8.56 (d, *J* = 4.2 Hz, $H^{6'}$ bipy^2, 1 H), 8.22 – 8.13 (m, $H^{4'}$ bipy^2 and $H^{4'}$ bipy^1, 2 H), 8.11 (d, *J* = 6.5 Hz, H^6 bipy^1, 1 H), 7.97 – 7.89 (m, H^4 bipy^1 and H^4 bipy^2, 2 H), 7.82 (ddd, *J* = 7.6, 5.7, 1.3 Hz, $H^{5'}$ bipy^1, 1 H), 7.76 – 7.69 (m, $H^{5'}$ bipy^2 and H^6 bipy^2, 2 H), 7.33 – 7.25 (m, H^5 bipy^1 and H^5 bipy^2, 2 H), 5.89 (d, *J* = 2.5 Hz, H^4 dmpzH, 1 H), 2.28 (s, $CH_3{}^5$ dmpzH, 3 H), 1.31 (s, $CH_3{}^3$ dmpzH, 3 H). ^{13}C NMR (126 MHz, Acetone-d_6) δ 160.23 (1C, C^2 bipy^1), 159.09 (1C, C^2 bipy^2), 158.33 (1C, $C^{2'}$ bipy^2), 158.23 (1C, $C^{2'}$ bipy^1), 153.66 (1C, C^6 bipy^1), 153.32 (1C, C^3 dmpzH), 153.08 (1C, $C^{6'}$ bipy^1), 152.79 (1C, $C^{6'}$ bipy^2), 152.11 (1C, C^6 bipy^2), 141.35 (1C, C^5 dmpzH), 136.22 (1C, C^4 bipy^2), 136.10 (2C, $C^{4'}$ bipy^1 and $C^{4'}$ bipy^2), 135.33 (1C, C^4 bipy^1), 126.61 (1C, C^5 bipy^2), 126.38 (1C, C^5 bipy^1), 126.26 (1C, $C^{5'}$ bipy^1), 126.11 (1C, $C^{5'}$ bipy^2), 123.60 (1C, C^3 bipy^2), 123.45 (1C, $C^{3'}$ bipy^2), 123.08 (1C, $C^{3'}$ bipy^1), 122.99 (1C, C^3 bipy^1), 107.84 (1C, C^4 dmpzH), 11.83 (1C, $CH_3{}^3$ dmpzH), 9.78 (1C, $CH_3{}^5$ dmpzH). ^{15}N NMR (51 MHz, Acetone-d_6) δ: −117.30 (1N, $N^{1'}$ bipy^2), −121.56 (1N, $N^{1'}$ bipy^1), −125.19 (1N, N^1 bipy^2), −126.75 (1N, N^1 bipy^1), −163.15 (1N, N^2 dmpzH), −173.61 (1N, N^1 dmpzH). IR (solid, cm^{-1}): 3302 m, 3078 w, 2287 w, 2051 w, 1981 w, 1602 w, 1570 m, 1461 m, 1444 m, 1420 m, 1373 w, 1255 vs, 1222 s, 1146 s, 1123 m, 1067 w, 1029 vs, 971 w, 895 w, 801 w, 785 w, 761 vs,728 s, 683 w, 658 w, 634 vs. Anal. Calcd for $C_{26}H_{24}ClF_3N_6O_3RuS$: C, 44.99; H, 3.49; N, 12.11; S, 4.62. Found: C, 44.95; H, 3.46; N, 12.02; S, 4.60.

***cis*-[Ru(bipy)$_2$(H$_2$O)(pzH)](OTf)$_2$, 2a.** AgOTf (0.128 g, 0.5 mmol) and 500 µL of distillated water were added to a solution of **1a** (0.333 g, 0.5 mmol) in Me_2CO (20 mL) and the mixture was stirred at r.t. for 24 h in the absence of light. The solution was filtered to remove solid AgCl and dried in vacuo. The red residue was crystallized in acetone/Et_2O at -20°C, giving a red microcrystalline solid, which was decanted, washed with Et_2O (3 x 5 mL approximately), and dried in vacuo, yielding 0.319 g (80%). ^{1}H NMR (500 MHz, Acetone-d_6) δ 9.51 (d, *J* = 5.5 Hz, $H^{6'}$ bipy^1, 1 H), 8.77 (d, *J* = 8.2 Hz, $H^{3'}$ bipy^2, 1 H), 8.69 (d, *J* = 5.6 Hz, $H^{6'}$ bipy^2, 1 H), 8.65 (m, $H^{3'}$ bipy^1 and H^3 bipy^2, 2 H), 8.54 (d, *J* = 8.1 Hz, H^3 bipy^1, 1 H), 8.29 – 8.19 (m, $H^{4'}$ bipy^2 and $H^{4'}$ bipy^1, 2 H), 8.03 – 7.96 (m, H^4 bipy^2 and H^6 bipy^1, 2 H), 7.96 – 7.87 (m, H^4 bipy^1, H^6 bipy^2, $H^{5'}$ bipy^1 and H^5 pzH, 4 H), 7.78 (t, *J* = 6.6 Hz, $H^{5'}$ bipy^2, 1 H), 7.38 – 7.29 (m, H^5 bipy^1, H^5 bipy^2 and H^3 pzH, 3 H), 6.44 (s, H^4 pzH, 1 H). ^{13}C NMR (126 MHz, acetone) δ 159.95 (1C, C^2 bipy^1), 458.91 (1C, $C^{2'}$ bipy^2), 158.30 (1C, C^2 bipy^2), 157.58 (1C, $C^{2'}$ bipy^1), 154.14 (1C, C^6 bipy^1), 153.24 (1C, $C^{6'}$ bipy^2), 153.08 (1C, C^6 bipy^2), 151.47 (1C, $C^{6'}$ bipy^1), 141.26 (1C, C^3 pzH), 137.73 (1C, C^4 bipy^1), 137.38 (1C, $C^{4'}$ bipy^2), 137.24 (1C, C^4 bipy^2), 136.16 (1C, $C^{4'}$ bipy^1), 132.86 (1C, C^5 pzH), 127.31 (1C, $C^{5'}$ bipy^1), 127.26 (1C, $C^{5'}$ bipy^2), 126.83 (1C, C^5 bipy^1), 126.55 (1C, C^5 bipy^2), 123.92 (1C, $C^{3'}$ bipy^2), 123.79 (1C, C^3 bipy^1), 123.61 (1C, $C^{3'}$ bipy^1), 123.52 (1C, C^3 bipy^2), 107.47 (1C, C^4 pzH). ^{15}N NMR

(51 MHz, Acetone-d_6) δ: −124.77 (1N, $N^{1'}$ $bipy^1$), −126.10 (1N, $N^{1'}$ $bipy^2$), −130.38 (1N, N^1 $bipy^2$), −134.49 (1N, N^1 $bipy^1$), −153.58 (1N, N^2 pzH), −174.07 (1N, N^1 pzH). IR (solid, cm^{-1}): 3251 m, 3113 m, 2324 w, 2164 w, 2113 w, 2051 w, 1981 w, 1605 m, 1529 w, 1486 m, 1467 m, 1426 m, 1358 w, 1314 vs, 1242 vs, 1155 vs, 1128 vs, 1064 w, 1050 m, 1028 vs, 970 m, 950 m, 909 m, 872 w, 759 vs, 730 vs, 661 w, 632 vs, 609 m. Anal. Calcd for **2a**·H_2O $C_{25}H_{22}F_6N_6O_7RuS_2$: C, 36.81; H, 2.97; N, 10.30; S, 7.86. Found: C, 36.77; H, 3.02; N, 9.73; S, 8.13.

***cis*-[Ru(bipy)$_2$(H$_2$O)(indzH)](OTf)$_2$, 2b.** The same procedure as for **2a**, using **1b** (0.358 g, 0.5 mmol) as starting material, gave 0.351 g (83%) of **2b** as a red microcrystalline solid. ^{1}H NMR (500 MHz, Acetone-d_6) δ 9.55 (d, J = 5.6 Hz, $H^{6'}$ $bipy^1$, 1 H), 8.82 – 8.76 (m, $H^{6'}$ $bipy^2$ and $H^{3'}$ $bipy^2$, 2 H), 8.66 (d, J = 8.2 Hz, H^3 $bipy^2$, 1 H), 8.63 (d, J = 8.1 Hz, $H^{3'}$ $bipy^1$, 1 H), 8.54 (d, J = 8.2 Hz, H^3 $bipy^1$, 1 H), 8.26 (t, J = 8.4 Hz, $H^{4'}$ $bipy^2$, 1 H), 8.20 (t, J = 7.5 Hz, $H^{4'}$ $bipy^1$, 1 H), 8.08 – 7.98 (m, H^3 indzH, H^4 $bipy^2$ and H^6 $bipy^1$, 3 H), 7.98 – 7.87 (m, H^4 $bipy^1$, H^6 $bipy^2$ and $H^{5'}$ $bipy^1$, 3 H), 7.73 (t, J = 7.3 Hz, $H^{5'}$ $bipy^2$, 1 H), 7.66 (d, J = 8.3 Hz, H^4 indzH, 1 H), 7.56 (d, J = 8.6 Hz, H^7 indzH, 1 H), 7.43 – 7.34 (m, H^6 indzH, H^5 $bipy^1$ and H^5 $bipy^2$, 3 H), 7.16 (t, J = 8.0 Hz, H^5 indzH, 1 H). ^{13}C NMR (126 MHz, acetone) δ 159.83 (1C, $C^{2'}$ $bipy^1$), 158.72 (1C, $C^{2'}$ $bipy^2$), 158.20 (1C, C^2 $bipy^2$), 157.49 (1C, C^2 $bipy^1$), 154.20 (1C, C^6 $bipy^1$), 153.27 (1C, $C^{6'}$ $bipy^2$), 152.94 (1C, C^6 $bipy^2$), 151.50 (1C, $C^{6'}$ $bipy^1$), 141.79 (1C, C^{7a} indzH), 137.92 (1C, $C^{4'}$ $bipy^2$), 137.63 (1C, $C^{4'}$ $bipy^1$), 137.49 (1C, C^3 indzH), 137.20 (1C, C^4 $bipy^2$), 136.44 (1C, C^4 $bipy^1$), 128.00 (1C, C^5 $bipy^1$), 127.44 (1C, $C^{5'}$ $bipy^1$), 127.32 (1C, $C^{5'}$ $bipy^2$), 127.01 (1C, C^5 $bipy^2$), 126.65 (1C, C^6 IndzH), 124.00 (1C, $C^{3'}$ $bipy^2$), 123.91 (1C, C^3 $bipy^1$), 123.68 (1C, $C^{3'}$ $bipy^1$), 123.58 (1C, C^3 $bipy^2$), 123.34 (1C, C^{3a} indzH), 122.00 (1C, C^5 indzH), 119.96 (1C, C^4 indzH), 110.10 (1C, C^7 indzH). ^{15}N NMR (51 MHz, Acetone-d_6) δ: −126.29 (1N, $N^{1'}$ $bipy^1$), −126.95 (1N, $N^{1'}$ $bipy^2$), −131.04 (1N, N^1 $bipy^2$), −135.68 (1N, N^1 $bipy^1$), −135.93 (1N, N^2 indzH), −197.76 (1N, N^1 indzH). IR (solid, cm^{-1}): 3235 m, 3117 m, 2324 w, 2164 w, 2051 w, 1981 w, 1626 m, 1605 m, 1568 w, 1509 w, 1466 m, 1426 m, 1385 w, 1357 w, 1222 vs, 1162 vs, 1125 vs, 1067 m, 1025 vs, 965 m, 902 w, 854 w, 840 w, 800 w, 763 vs, 729 s, 661 w, 632 vs. Anal. Calcd for **2b**·H_2O $C_{29}H_{24}F_6N_6O_7RuS_2$: C, 40.23; H, 3.03; N, 9.71; S, 7.41. Found: C, 39.89; H, 2.83; N, 9.46; S, 7.68.

***cis*-[Ru(bipy)$_2$(H$_2$O)(dmpzH)](OTf)$_2$, 2c.** The same procedure as for **2a**, using **1c** (0.347 g, 0.5 mmol) as starting material, gave 0.310 g (78%) of **2c** as a red microcrystalline solid. ^{1}H NMR (500 MHz, Acetone-d_6) δ 9.71 (d, J = 5.3 Hz, $H^{6'}$ $bipy^1$, 1 H), 8.83 (m, $H^{6'}$ $bipy^2$ and $H^{3'}$ $bipy^2$, 2 H), 8.69 (m, $H^{3'}$ $bipy^1$ and H^3 $bipy^2$, 2 H), 8.57 (d, J = 8.0 Hz, H^3 $bipy^1$, 1 H), 8.29 (td, J = 8.0, 1.4 Hz, $H^{4'}$ $bipy^2$, 1 H), 8.25 (td, J = 8.0, 1.4 Hz, $H^{4'}$ $bipy^1$, 1 H), 8.09 (d, J = 5.7 Hz, H^6 $bipy^1$, 1 H), 8.01 (td,

J = 8.0, 1.4 Hz, H^4 bipy^2, 1 H), 7.96 – 7.86 (m, H^4 bipy^1, H^6 bipy^2 and $H^{5'}$ bipy^1, 4 H), 7.82 (ddd, *J* = 7.4, 5.6, 1.2 Hz, $H^{5'}$ bipy^2, 1 H), 7.34 (ddd, *J* = 7.4, 5.7, 1.3 Hz, H^5 bipy^2, 1 H), 7.28 (ddd, *J* = 7.3, 5.8, 1.3 Hz, H^5 bipy^1, 1 H), 5.97 (s, H^4 dmpzH, 1 H), 2.26 (s, $CH_3{}^5$ dmpzH, 3 H), 1.48 (s, $CH_3{}^3$ dmpzH, 3 H). ^{13}C NMR (126 MHz, acetone) δ 160.28 (1C, C^2 bipy^1), 159.09 (1C, C^2 bipy^2), 158.48 (1C, $C^{2'}$ bipy^2), 157.78 (1C, $C^{2'}$ bipy^1), 154.77 (1C, C^6 bipy^1), 153.88 (2C, $C^{6'}$ bipy^2 and C^3 dmpzH), 153.51 (1C, C^6 bipy^2), 152.23 (1C, $C^{6'}$ bipy^1), 143.19 (1C, C^5 dmpzH), 137.80 (1C, $C^{4'}$ bipy^2), 137.28 (2C, $C^{4'}$ bipy^1 and C^4 bipy^2), 135.94 (1C, C^4 bipy^1), 127.25 (1C, $C^{5'}$ bipy^2), 127.04 (1C, $C^{5'}$ bipy^1), 126.59 (1C, C^5 bipy^2), 126.17 (1C, C^5 bipy^1), 124.09 (1C, $C^{3'}$ bipy^2), 123.64 (1C, $C^{3'}$ bipy^1), 123.59 (1C, C^3 bipy^1), 123.48 (1C, C^3 bipy^2), 108.18 (1C, C^4 dmpzH), 12.56 (1C, $CH_3{}^3$ dmpzH), 9.89 (1C, $CH_3{}^5$ dmpzH). ^{15}N NMR (51 MHz, Acetone-d_6) δ: −124.96 (1N, $N^{1'}$ bipy^2), −126.46 (1N, $N^{1'}$ bipy^2), −130.52 (1N, N^1 bipy^2), −132.89 (1N, N^1 bipy^1), −164.13 (1N, N^2 dmpzH), −180.07 (1N, N^1 dmpzH). IR (solid, cm^{-1}): 3340 m, 3116 w, 3084 w, 2324 w, 2164 w, 2051 w, 1981 w, 1605 m, 1574 m, 1486 w, 1466 m, 1447 m, 1425 m, 1382 w, 1251 vs, 1150 vs, 1029 vs, 799 w, 787 m, 761 s, 729 s, 660 w, 631 vs. Anal. Calcd for **2c**·H2O $C_{27}H_{26}F_6N_6O_7RuS_2$: C, 38.44; H, 3.35; N, 9.96; S, 7.60. Found: C, 38.26; H, 3.25; N, 9.35; S, 8.09.

***cis*-[Ru(bipy)$_2$(indzH)$_2$](PF$_6$)$_2$, 3.** A mixture of *cis*-[Ru(bipy)$_2$Cl$_2$]·2H$_2$O (0.107 g, 0.2 mmol), indzH (0.052 g, 0.44 mmol) and H$_2$O (10 mL) was refluxed for 2.30 h. Then NH_4PF_6 (0.326 g, 2 mmol) was added and an orange precipitate appears. The precipitate was filtered off and washed with Et_2O (3 × 5 mL approximately), and dried, yielding 0.167 g, 84%. ^{1}H RMN ((CD$_3$)$_2$SO, r,t.) δ: 13.10 (s, H^1 indzH, 2 H), 9.23 (d, J = 7 Hz, H^5 indzH, 2 H), 8.62 (d, H^3 indzH, 2H), 8.56 (d, J = 8 Hz, H^6 bipy, 2 H), 8.19 (m, H^7 indzH and $H^{6'}$ bipy, 4 H), 8.00 (m, $H^{3'}$ bipy, 2 H), 7.92 (d, H^3 bipy, 2 H), 7.87 (m, H^4 indzH, 2 H), 7.66 (d, J = 7 Hz, H^6 indzH, 2 H), 7.49 (m, H^5 bipy, 2 H), 7.38 (m, H^4 y $H^{4'}$ bipy, 4 H), 7.14 (m, $H^{5'}$ bipy, 2 H). ^{13}C {^{1}H} RMN ((CD$_3$)$_2$SO, r.t.) δ: 157.6 (2C, $C^{2'}$ bipy), 157.03 (2C, C^2 bipy), 156.9 (2C, C^{7a} indzH), 153.8 (2C, C^5 indzH), 152.9 (2C, C^6 bipy), 142.3 (2C, C^{3a} indzH), 138.7 (2C, C^7 indzH), 138.4 (2C, $C^{6'}$bipy), 138.1 (2C, C^4 bipy), 128.2 (2C, $C^{4'}$ bipy), 127.9 (2C, C^5 bipy), 127.8 (2C, C^6 indzH), 124.2 (2C, $C^{5'}$ bipy), 123.3 (2C, C^3 indzH), 122.2 (2C, C^3 bipy), 120.5 (2C, C^4 indzH), 110.3 (2C, $C^{3'}$ bipy). IR (cm^{-1}): 3642 w, 3573 w, 3431 w, 3126 w, 2323 w, 2163 w, 2139 w, 2111 w, 2050 w, 1980 w, 1938 w, 1627 m, 1603 m, 1510 w, 1466 m, 1444 s, 1423 m, 1385 w, 1359 s, 1326 w, 1313 w, 1274 m, 1244 w, 1223 w, 1153 w, 1129 w, 1076 w, 1026 w, 1004 w, 967 w, 942 w, 902 w, 826 vs, 758 vs, 731 vs, 660 w, 617 w. Anal. Calcd for **3**·4MeCN, $C_{42}H_{40}F_{12}N_{12}P_2Ru$: C, 45.23; H, 3.40; N, 15.61. Found: C, 45.69; H, 3.65; N, 15.23.

Photophysical experiments. The solvents for spectroscopic studies were of spectroscopic grade and used as received. Ultraviolet–visible (UV–Vis) and fluorescence spectra were recorded in optically dilute solutions (from 1×10^{-5} M to 5×10^{-5} M), at room temperature with a quartz cuvette (1 cm×1 cm), using a Hitachi U-3900 and an F-7000 Hitachi Fluorescence spectrophotometers, respectively. Fluorescence decay lifetimes were measured in deaerated solvents, using a time-correlated single photon counting instrument (FLS980 Series, Edinburgh instruments) with a 405 nm pulsed LED (Edinburgh instruments, EPL-510) light source having a 50–500 ns. The absolute fluorescence quantum yields in each solvent were measured using the integrating sphere accessory with a FLS980 Series Edinburgh instrument, wherein the solvent was used as a reference. χ^2 is a stadistic parameter which accounts for the quality of fit between the observed and the model exponential decays (ideal value = 1). Tail fits and numerical reconvolution were obtained by using FAST software package (Edinburgh Instruments).

Electrochemical experiments. Electrochemical measurements were carried out with Dropsens µStat 400 (range −4V to +4V, software DropView 8400 Version 2.2), or Dropsens Stat 300 (range −2V to +2V) or PalmSens 3 potentiostats (range −5V to +5V, software PSTrace4 Version 4.4.2). Unless otherwise stated CV's were scanned at 200 mVs^{-1}, in acetonitrile (5 ml), 0.1M n-Bu_4PF_6 supporting electrolyte, purging with Ar or CO_2 at room temperature through a PTFE tubing. Working electrodes were of glassy carbon (3 mm diameter). The auxiliary electrode was a platinum wire. The reference electrodes used were Ag/AgCl (3M NaCl) MF-2052 BASi (separated from the bulk solution by a "thirsty" Vycor™ frit) or a silver wire pseudo-reference electrode. Ferrocene was added at the end of the experiments. The observed ferrocenium/ferrocene couple was $E_{1/2}$ = 0.443±0.005 V vs. Ag/AgCl. Potential values measured with the Ag wire are plenty of uncertainty and, at the end of the experiment, measures must be carried out with the Ag/AgCl (3M NaCl) electrode.

The solubility of saturated CO_2 in acetonitrile has been reported to be 0.28M at 25°C.[72,73] Changing atmosphere from pure Ar to pure CO_2 or vice versa required bubbling with the new gas for not less than five minutes. Lasting such time, the CV's obtained were the same than those obtained in the first scan under a specific atmosphere. Bubbling was kept during

the interim between scans. During scan time the PTFE was risen and kept above the surface of the solution to avoid agitation.

Controlled potential electrolysis. Controlled potential electrolysis (CPE) studies of the complexes (1mM) were carried out in CH_3CN with 0.1 M $TBAPF_6$ as the electrolyte and at −2.7V vs the Fc^+/Fc couple for 2 h using a model CHI6012D electrochemical workstation. CPE studies were performed in a specialized three compartment cell using a three-electrode set-up which consisting of a glassy carbon working electrode, a $Ag/AgNO_3$ reference electrode and a platinum wire counter electrode. The solution was saturated with CO_2 (that had been dried by passing through 5 Å molecular sieves) for 30 minutes after which it was made airtight and then CPE initiated.

Product analysis was accomplished according to the nature of the product, *i.e.* gas or liquid. The gaseous products were then analyzed by sampling the headspace of the electrolysis cell using a gas tight Hamilton 1001 SL SYR, syringe at the conclusion of electrochemical runs. The analysis was achieved by a Shimadzu GC2014 gas chromatograph equipped with 60/80 CARBOXEN-1000 15' x 1/8" SS (2.1 mm I.D.) column. For the gaseous sample analysis, a 0.5 mL sample of the gas was injected via the on-column injector by the gas tight Hamilton syringe. The carrier gas used was helium. The determination of formic acid was accomplished using ^1H NMR spectroscopy by a previously reported method.[66] Briefly, to quantify the amount of formic acid in the bulk electrolysis samples, a calibration curve for formic acid was prepared using an internal standard of dimethyl sulfone in a solvent of D_2O. Thereafter 150 µL of the bulk electrolysis sample was extracted and subsequently mixed with 600 µL of dimethyl sulfone in a solvent of D_2O. The mixture was then sonicated for 1 minute and 400 µL placed in an NMR tube and ^1H NMR spectra subsequently recorded. The integration value(s) for the peak at 8.5 ppm was recorded and with reference to the calibration curve previously established, the formic acid generated in each sample was quantified.

Photocatalysis Procedure. A 20 ml vial containing 0.1mM catalyst and 1.6mM $[Ru(bipy)_3]^{2+}$ was added a solvent mixture of CH_3CN-TEOA (5:1 v/v) to afford a total volume of 10 ml. Subsequently the vial was sealed with a rubber septum and the solution was bubbled with CO_2 for 20 minutes. The CO_2 saturated solution was thereafter irradiated with a 150W EKE Kramer scientific corporation modulamp, light source having a UV-cut filter (>300nm). After conclusion

of the photochemical run the head space was sampled using a gas tight Hamilton 1001 SL SYR, syringe. The head space gas analysis was then accomplished using a SHIMADZU GC2014 gas chromatograph equipped with 60/80 CARBOXEN-1000 15' x1/8" SS (2.1 mm I.D.) column. The quantum yields (QY) of the evolution of HCOOH and CO by the complexes under study were determined according to a previously established protocol.[74]

Crystal Structure Determination for Compounds 1a, 1b, 2b and 2c. Crystals were grown in concentrated solutions of the complexes in methanol (for **1a** and **1b**) at −20 °C, or by slow diffusion of Et_2O into concentrated solutions of the complexes in acetone (for **2b** and **2c**) at −20 °C. Relevant crystallographic details can be found in the CIF. A crystal was attached to a glass fiber and transferred to an Agilent SuperNova diffractometer fitted with an Atlas CCD detector. The crystals were kept at 293(2) K during data collection. Using Olex2,[75] the structures were solved with the ShelXT[76] structure solution program and then the structures were refined with the ShelXL[77] refinement package using least squares minimization. All non-hydrogen atoms were refined anisotropically. Hydrogen atoms were set in calculated positions and refined as riding atoms, with a common thermal parameter. All graphics were made with Olex2, and distances and angles of hydrogen bonds were calculated with PARST[78,79] (normalized values).[80,81]

ASSOCIATED CONTENT

The Supporting Information is available free of charge at https://pubs.acs.org/doi/...:

Cyclic Voltammograms (Figures S1 to S22) of complexes **1**-**4**. Normalized UV/vis absorption and emission spectra (Figure S23) of complexes **1** and **2**, and emission spectra of **1c** and **2c** in aerated and deaerated MeCN (Figure S24). Photocatalytic experiments (Figures S25 and S26) of complexes **1** and **2**. ^{1}H NMR spectrum of the photochemical solution of **1c** indicating the formate chemical shift (Figure S27).

Crystal structures of complexes **1a**, **1b**, **2a** and **2c**. CCDC 2031192-2031195 contain the supplementary crystallographic data for this paper. These data can be obtained free of charge via www.ccdc.cam.ac.uk/data_request/cif, or by emailing data_request@ccdc.cam.ac.uk, or by

contacting The Cambridge Crystallographic Data Centre, 12 Union Road, Cambridge CB2 1EZ, UK; fax: +44 1223 336033.

AUTHOR INFORMATION

Corresponding Author

Fernando Villafañe. GIR MIOMeT-IU Cinquima-Química Inorgánica, Facultad de Ciencias, Campus Miguel Delibes, Universidad de Valladolid, 47011 Valladolid, Spain. orcid.org/0000-0002-3230-3802. E-mail: fernando.villafane@uva.es

Authors

Elena Cuéllar. GIR MIOMeT-IU Cinquima-Química Inorgánica, Facultad de Ciencias, Campus Miguel Delibes, Universidad de Valladolid, 47011 Valladolid, Spain. orcid.org/0000-0002-1766-1230

Laura Pastor. GIR MIOMeT-IU Cinquima-Química Inorgánica, Facultad de Ciencias, Campus Miguel Delibes, Universidad de Valladolid, 47011 Valladolid, Spain.

Gabriel García-Herbosa. Departamento de Química, Facultad de Ciencias, Universidad de Burgos, 09001 Burgos, Spain. orcid.org/0000-0002-2863-1272

John Nganga. Department of Chemistry, University of Connecticut, 55 N. Eagleville Rd, Storrs, CT 06269, USA.

Alfredo M. Angeles-Boza. Department of Chemistry, University of Connecticut, 55 N. Eagleville Rd, Storrs, CT 06269, USA. Institute of Materials Science, University of Connecticut, 97 N. Eagleville Rd, Storrs, CT 06269, USA. orcid.org/0000-0002-5560-4405

Alberto Diez-Varga. Departamento de Química, Facultad de Ciencias, Universidad de Burgos, 09001 Burgos, Spain.

Tomás Torroba. Departamento de Química, Facultad de Ciencias, Universidad de Burgos, 09001 Burgos, Spain. orcid.org/0000-0002-5018-4173

Jose M. Martín-Alvarez. GIR MIOMeT-IU Cinquima-Química Inorgánica, Facultad de Ciencias, Campus Miguel Delibes, Universidad de Valladolid, 47011 Valladolid, Spain. orcid.org/0000-0002-6969-0703

Daniel Miguel. GIR MIOMeT-IU Cinquima-Química Inorgánica, Facultad de Ciencias, Campus Miguel Delibes, Universidad de Valladolid, 47011 Valladolid, Spain. orcid.org/0000-0003-0650-3058

Author Contributions

The manuscript was written through contributions of all authors. All authors have given approval to the final version of the manuscript.

Notes

The authors declare no competing financial interest.

ACKNOWLEDGMENTS

This research was supported by the Junta de Castilla y León (Ref. VA130618). E. C. thanks the UVa for her grant. The authors in Valladolid gratefully acknowledge financial support from the Spanish MINECO, Spain (PGC2018-099470-B-I00) and Junta de Castilla y León (VA130618), and the authors in Burgos gratefully acknowledge financial support from the Junta de Castilla y León, Consejería de Educación y Cultura and Fondo Social Europeo (Project BU263P18). A.M.A.-B. is grateful for support from the National Science Foundation CAREER grant (CHE-1652606).

REFERENCES

(1) Takeda, H.; Ishitani, O. Development of Efficient Photocatalytic Systems for CO2 Reduction Using Mononuclear and Multinuclear Metal Complexes Based on Mechanistic Studies. *Coord. Chem. Rev.* **2010**, *254* (3–4), 346–354.

(2) Qiao, J.; Liu, Y.; Hong, F.; Zhang, J. A Review of Catalysts for the Electroreduction of Carbon Dioxide to Produce Low-Carbon Fuels. *Chem. Soc. Rev.* **2014**, *43* (2), 631–675.

(3) Elgrishi, N.; Chambers, M. B.; Wang, X.; Fontecave, M. Molecular Polypyridine-Based Metal Complexes as Catalysts for the Reduction of CO2. *Chem. Soc. Rev.* **2017**, *46* (3), 761–796.

(4) Francke, R.; Schille, B.; Roemelt, M. Homogeneously Catalyzed Electroreduction of Carbon Dioxide—Methods, Mechanisms, and Catalysts. *Chem. Rev.* **2018**, *118* (9), 4631–4701.

(5) Kuramochi, Y.; Ishitani, O.; Ishida, H. Reaction Mechanisms of Catalytic Photochemical CO2 Reduction Using Re(I) and Ru(II) Complexes. *Coord. Chem. Rev.* **2018**, *373*, 333–356.

(6) Jiang, C.; Nichols, A. W.; Machan, C. W. A Look at Periodic Trends in D-Block Molecular Electrocatalysts for CO2 Reduction. *Dalton Trans.* **2019**, *48* (26), 9454–9468.

(7) Luo, Y.-H.; Dong, L.-Z.; Liu, J.; Li, S.-L.; Lan, Y.-Q. From Molecular Metal Complex to Metal-Organic Framework: The CO2 Reduction Photocatalysts with Clear and Tunable Structure. *Coord. Chem. Rev.* **2019**, *390*, 86–126.

(8) Yamazaki, Y.; Takeda, H.; Ishitani, O. Photocatalytic Reduction of CO2 Using Metal Complexes. *J. Photochem. Photobiol. C Photochem. Rev.* **2015**, *25*, 106–137.

(9) Ishida, H.; Tanaka, K.; Tanaka, T. Electrochemical CO2 Reduction Catalyzed by [Ru(Bpy)2(CO)2]2+ and [Ru(Bpy)2(CO)Cl]+ . The Effect of PH on the Formation of CO and HCOO-. *Organometallics* **1987**, *6* (1), 181–186.

(10) Voyame, P.; Toghill, K. E.; Méndez, M. A.; Girault, H. H. Photoreduction of CO2 Using [Ru(Bpy)2(CO)L]n+ Catalysts in Biphasic Solution/Supercritical CO2 Systems. *Inorg. Chem.* **2013**, *52* (19), 10949–10957.

(11) Ishida, H.; Tanaka, H.; Tanaka, K.; Tanaka, T. Electrochemical Reaction of CO2 with Me2NH to Afford N , N -Dimethylformamide, Catalyzed by [Ru(Bpy)2(CO)2]2+ (Bpy = 2,2′-Bipyridine). *Chem. Lett.* **1987**, *16* (4), 597–600.

(12) Ishida, H.; Tanaka, H.; Tanaka, K.; Tanaka, T. Selective Formation of HCOO – in the Electrochemical CO2 Reduction Catalysed by [Ru(Bpy)2(CO)2]2+ (Bpy = 2,2′-Bipyridine). *J. Chem. Soc., Chem. Commun.* **1987**, No. 2, 131–132.

(13) Tanaka, K.; Morimoto, M.; Tanaka, T. The Water Gas Shift Reaction Catalyzed By Ruthenium Carbonyl Complexes. *Chem. Lett.* **1983**, *12* (6), 901–904.

(14) Pugh, J. R.; Bruce, M. R. M.; Sullivan, B. P.; Meyer, T. J. Formation of a Metal-Hydride

Bond and the Insertion of CO2. Key Steps in the Electrocatalytic Reduction of Carbon Dioxide to Formate Anion. *Inorg. Chem.* **1991**, *30* (1), 86–91.

(15) Sullivan, B. P.; Meyer, T. J. Photoinduced Irreversible Insertion of CO2 into a Metal–Hydride Bond. *J. Chem. Soc., Chem. Commun.* **1984**, No. 18, 1244–1245.

(16) Sullivan, B. P.; Caspar, J. V.; Meyer, T. J.; Johnson, S. Hydrido Carbonyl Complexes of Osmium(II) and Ruthenium(II) Containing Polypyridyl Ligands. *Organometallics* **1984**, *3* (8), 1241–1251.

(17) Hawecker, J.; Lehn, J.-M.; Ziessel, R. Photochemical and Electrochemical Reduction of Carbon Dioxide to Carbon Monoxide Mediated by (2,2'-Bipyridine)Tricarbonylchlororhenium(I) and Related Complexes as Homogeneous Catalysts. *Helv. Chim. Acta* **1986**, *69* (8), 1990–2012.

(18) Lehn, J.-M.; Ziessel, R. Photochemical Reduction of Carbon Dioxide to Formate Catalyzed by 2,2ŧ-Bipyridine- or 1,10-Phenanthroline-Ruthenium(II) Complexes. *J. Organomet. Chem.* **1990**, *382* (1–2), 157–173.

(19) Sampaio, R. N.; Grills, D. C.; Polyansky, D. E.; Szalda, D. J.; Fujita, E. Unexpected Roles of Triethanolamine in the Photochemical Reduction of CO2 to Formate by Ruthenium Complexes. *J. Am. Chem. Soc.* **2020**, *142* (5), 2413–2428.

(20) Kuramochi, Y.; Kamiya, M.; Ishida, H. Photocatalytic CO 2 Reduction in N , N -Dimethylacetamide/Water as an Alternative Solvent System. *Inorg. Chem.* **2014**, *53* (7), 3326–3332.

(21) Nagao, H.; Mizukawa, T.; Tanaka, K. Carbon-Carbon Bond Formation in the Electrochemical Reduction of Carbon Dioxide Catalyzed by a Ruthenium Complex. *Inorg. Chem.* **1994**, *33* (15), 3415–3420.

(22) Chen, Z.; Chen, C.; Weinberg, D. R.; Kang, P.; Concepcion, J. J.; Harrison, D. P.; Brookhart, M. S.; Meyer, T. J. Electrocatalytic Reduction of CO2 to CO by Polypyridyl Ruthenium Complexes. *Chem. Commun.* **2011**, *47* (47), 12607–12609.

(23) Chen, Z.; Kang, P.; Zhang, M. T.; Meyer, T. J. Making Syngas Electrocatalytically Using a Polypyridyl Ruthenium Catalyst. *Chem. Commun.* **2014**, *50* (3), 335–337.

(24) Duan, L.; Manbeck, G. F.; Kowalczyk, M.; Szalda, D. J.; Muckerman, J. T.; Himeda, Y.; Fujita, E. Noninnocent Proton-Responsive Ligand Facilitates Reductive Deprotonation and Hinders CO2 Reduction Catalysis in [Ru(Tpy)(6DHBP)(NCCH3)]2+ (6DHBP = 6,6'-(OH)2bpy). *Inorg. Chem.* **2016**, *55* (9), 4582–4594.

(25) Johnson, B. A.; Maji, S.; Agarwala, H.; White, T. A.; Mijangos, E.; Ott, S. Activating a Low Overpotential CO2 Reduction Mechanism by a Strategic Ligand Modification on a Ruthenium Polypyridyl Catalyst. *Angew. Chemie Int. Ed.* **2016**, *55* (5), 1825–1829.

(26) Johnson, B. A.; Agarwala, H.; White, T. A.; Mijangos, E.; Maji, S.; Ott, S. Judicious Ligand Design in Ruthenium Polypyridyl CO2 Reduction Catalysts to Enhance Reactivity by Steric and Electronic Effects. *Chem. - A Eur. J.* **2016**, *22* (42), 14870–14880.

(27) White, T. A.; Maji, S.; Ott, S. Mechanistic Insights into Electrocatalytic CO_2 Reduction within $[Ru^{II}(Tpy)(NN)X]^{n+}$ Architectures. *Dalton Trans.* **2014**, *43* (40), 15028–15037.

(28) Schneider, T. W.; Hren, M. T.; Ertem, M. Z.; Angeles-Boza, A. M. [RuII(Tpy)(Bpy)Cl]+-

Catalyzed Reduction of Carbon Dioxide. Mechanistic Insights by Carbon-13 Kinetic Isotope Effects. *Chem. Commun.* **2018**, *54* (61), 8518–8521.

(29) Lee, S. K.; Kondo, M.; Nakamura, G.; Okamura, M.; Masaoka, S. Low-Overpotential CO2 Reduction by a Phosphine-Substituted Ru(II) Polypyridyl Complex. *Chem. Commun.* **2018**, *54* (50), 6915–6918.

(30) Lee, S. K.; Kondo, M.; Okamura, M.; Enomoto, T.; Nakamura, G.; Masaoka, S. Function-Integrated Ru Catalyst for Photochemical CO2 Reduction. *J. Am. Chem. Soc.* **2018**, *140* (49), 16899–16903.

(31) Gonell, S.; Massey, M. D.; Moseley, I. P.; Schauer, C. K.; Muckerman, J. T.; Miller, A. J. M. The Trans Effect in Electrocatalytic CO2 Reduction: Mechanistic Studies of Asymmetric Ruthenium Pyridyl-Carbene Catalysts. *J. Am. Chem. Soc.* **2019**, *141* (16), 6658–6671.

(32) Huang, J.; Chen, J.; Gao, H.; Chen, L. Kinetic Aspects for the Reduction of CO2 and CS2 with Mixed-Ligand Ruthenium(II) Hydride Complexes Containing Phosphine and Bipyridine. *Inorg. Chem.* **2014**, *53* (18), 9570–9580.

(33) Vos, J. G. Excited-State Acid-Base Properties of Inorganic Compounds. *Polyhedron* **1992**, *11* (18), 2285–2299.

(34) Rommel, S. A.; Sorsche, D.; Fleischmann, M.; Rau, S. Optical Sensing of Anions via Supramolecular Recognition with Biimidazole Complexes. *Chem. - A Eur. J.* **2017**, *23* (72), 18101–18119.

(35) Meng, T.-T.; Wang, H.; Zheng, Z.-B.; Wang, K.-Z. PH-Switchable "Off–On–Off" Near-Infrared Luminescence Based on a Dinuclear Ruthenium(II) Complex. *Inorg. Chem.* **2017**, *56* (9), 4775–4779.

(36) Viere, E. J.; Kuhn, A. E.; Roeder, M. H.; Piro, N. A.; Kassel, W. S.; Dudley, T. J.; Paul, J. J. Spectroelectrochemical Studies of a Ruthenium Complex Containing the PH Sensitive 4,4′-Dihydroxy-2,2′-Bipyridine Ligand. *Dalton Trans.* **2018**, *47* (12), 4149–4161.

(37) Brown, R. T.; Fletcher, N. C.; Danos, L.; Halcovitch, N. R. A Tripodal Ruthenium(II) Polypyridyl Complex with PH Controlled Emissive Quenching. *Eur. J. Inorg. Chem.* **2019**, *2019* (1), 110–117.

(38) Zhang, Z.-H.; He, P.; Kang, S.-R.; Liu, C.; Yi, X.-Y. Reversible Pyrrole-Based Proton Storage/Release in Ruthenium(II) Complexes. *Chem. Commun.* **2019**, *55* (97), 14594–14597.

(39) Swords, W. B.; Li, G.; Meyer, G. J. Iodide Ion Pairing with Highly Charged Ruthenium Polypyridyl Cations in CH3CN. *Inorg. Chem.* **2015**, *54* (9), 4512–4519.

(40) Troian-Gautier, L.; Beauvilliers, E. E.; Swords, W. B.; Meyer, G. J. Redox Active Ion-Paired Excited States Undergo Dynamic Electron Transfer. *J. Am. Chem. Soc.* **2016**, *138* (51), 16815–16826.

(41) Ghosh, T. K.; Chakraborty, S.; Chowdhury, B.; Ghosh, P. Bis-Heteroleptic Ruthenium(II) Complex of Pendant Urea Functionalized Pyridyl Triazole and Phenathroline for Recognition, Sensing, and Extraction of Oxyanions. *Inorg. Chem.* **2017**, *56* (9), 5371–5382.

(42) Pannwitz, A.; Poirier, S.; Bélanger-Desmarais, N.; Prescimone, A.; Wenger, O. S.; Reber,

C. Controlling Second Coordination Sphere Effects in Luminescent Ruthenium Complexes by Means of External Pressure. *Chem. - A Eur. J.* **2018**, *24* (31), 7830–7833.

(43) Sorsche, D.; Rommel, S. A.; Rau, S. Functional Dimming of Pincer-Shaped Bibenzimidazole-Ruthenium(II) Complexes with Improved Anion-Sensitive Luminescence. *Eur. J. Inorg. Chem.* **2016**, *2016* (10), 1503–1513.

(44) Han, M.-J.; Chen, Y.-M.; Wang, K.-Z. Ruthenium(Ii) Complexes of 6-Hydroxydipyrido[3,2-a:2′,3′-c]Phenazine: Self-Association, and Concentration-Dependent Acid–Base and DNA-Binding Properties. *New J. Chem.* **2008**, *32* (6), 970.

(45) Zheng, Z.-B.; Kang, S.-Y.; Yi, X.; Zhang, N.; Wang, K.-Z. Off–on–off PH Luminescence Switching and DNA Binding Properties of a Free Terpyridine-Appended Ruthenium Complex. *J. Inorg. Biochem.* **2014**, *141*, 70–78.

(46) Sullivan, B. P.; Salmon, D. J.; Meyer, T. J.; Peedin, J. Monomeric and Dimeric Pyrazole and Pyrazolyl Complexes of Ruthenium. *Inorg. Chem.* **1979**, *18* (12), 3369–3374.

(47) Hirahara, M.; Nakano, H.; Uchida, K.; Yamamoto, R.; Umemura, Y. Intramolecular Hydrogen Bonding: A Key Factor Controlling the Photosubstitution of Ruthenium Complexes. *Inorg. Chem.* **2020,** *59* (16), 11273-11286.

(48) Jude, H.; Rein, F. N.; Chen, W.; Scott, B. L.; Dattelbaum, D. M.; Rocha, R. C. Pyrazole and Pyrazolyl Complexes of Cis-Bis(2,2′-Bipyridine)- Chlororuthenium(II): Synthesis, Structural and Electronic Characterization, and Acid-Base Chemistry. *Eur. J. Inorg. Chem.* **2009**, No. 5, 683–690.

(49) Sá, D. S.; Fernandes, A. F.; Silva, C. D. S.; Costa, P. P. C.; Fonteles, M. C.; Nascimento, N. R. F.; Lopes, L. G. F.; Sousa, E. H. S. Non-Nitric Oxide Based Metallovasodilators: Synthesis, Reactivity and Biological Studies. *Dalton Trans.* **2015**, *44* (30), 13633–13640.

(50) Arroyo, M.; Miguel, D.; Villafañe, F.; Nieto, S.; Pérez, J.; Riera, L. Rhenium-Mediated Coupling of Acetonitrile and Pyrazoles. New Molecular Clefts for Anion Binding. *Inorg. Chem.* **2006**, *45* (17), 7018–7026.

(51) Gómez-Iglesias, P.; Guyon, F.; Khatyr, A.; Ulrich, G.; Knorr, M.; Martín-Alvarez, J. M.; Miguel, D.; Villafañe, F. Luminescent Rhenium(I) Tricarbonyl Complexes with Pyrazolylamidino Ligands: Photophysical, Electrochemical, and Computational Studies. *Dalton Trans.* **2015**, *44* (40), 17516–17528.

(52) Merillas, B.; Cuéllar, E.; Diez-Varga, A.; Asensio-Bartolomé, M.; García-Herbosa, G.; Torroba, T.; Martín-Alvarez, J. M.; Miguel, D.; Villafañe, F. Whole Microwave Syntheses of Pyridylpyrazole and of Re and Ru Luminescent Pyridylpyrazole Complexes. *Inorg. Chim. Acta* **2019**, *484*, 1–7.

(53) Merillas, B.; Cuéllar, E.; Diez-Varga, A.; Torroba, T.; García-Herbosa, G.; Fernández, S.; Lloret-Fillol, J.; Martín-Alvarez, J. M.; Miguel, D.; Villafañe, F. Luminescent Rhenium(I)Tricarbonyl Complexes Containing Different Pyrazoles and Their Successive Deprotonation Products: CO2 Reduction Electrocatalysts. *Inorg. Chem.* **2020**, *59* (15), 11152–11165.

(54) Kollipara, M. R.; Sarkhel, P.; Chakraborty, S.; Lalrempuia, R. Synthesis, Characterization and Molecular Structure of a New (η6-p-Cymene) Ruthenium(II) Amidine Complex, [(η6-p-Cymene)Ru{NH=C(Me)3,5-Dmpz}(3,5-Hdmpz)](BF4) 2·H2O. *J. Coord. Chem.* **2003**, *56* (12), 1085–1091.

(55) Schlapp-Hackl, I.; Hassenrück, C.; Wurst, K.; Kopacka, H.; Müller, T.; Winter, R. F.; Bildstein, B. Metallo-Scorpionates: First Generation of Trimetallic, Homoleptic [Ru]-M-[Ru] Complexes (M = Fe, Co, Ni, Cu). *Eur. J. Inorg. Chem.* **2018**, *2018* (40), 4434–4441.

(56) Gritzner, G.; Kuta, J. Recommendations on Reporting Electrode Potentials in Nonaqueous Solvents (Recommendations 1983). *Pure Appl. Chem.* **1984**, *56* (4), 461–466.

(57) Rapp, T. L.; Phillips, S. R.; Dmochowski, I. J.; Field, C.; Field, L. Kinetics and Photochemistry of Ruthenium Bisbipyridine Diacetonitrile Complexes: An Interdisciplinary Inorganic and Physical Chemistry Laboratory Exercise. *J. Chem. Educ.* **2016**, *93*, 2101–2105.

(58) Aranzaes, J. R.; Daniel, M.-C.; Astruc, D. Metallocenes as References for the Determination of Redox Potentials by Cyclic Voltammetry - Permethylated Iron and Cobalt Sandwich Complexes, Inhibition by Polyamine Dendrimers, and the Role of Hydroxy-Containing Ferrocenes. *Can. J. Chem.* **2006**, *84* (2), 288–299.

(59) Sullivan, B. P.; Conrad, D.; Meyer, T. J. Chemistry of Highly Reduced Polypyridyl-Metal Complexes. Anion Substitution Induced by Ligand-Based Reduction. *Inorg. Chem.* **1985**, *24* (22), 3640–3645.

(60) Costentin, C.; Robert, M.; Savéant, J.-M. Concerted Proton−Electron Transfers: Electrochemical and Related Approaches. *Acc. Chem. Res.* **2010**, *43* (7), 1019–1029.

(61) Liu, F.; Concepcion, J. J.; Jurss, J. W.; Cardolaccia, T.; Templeton, J. L.; Meyer, T. J. Mechanisms of Water Oxidation from the Blue Dimer to Photosystem II. *Inorg. Chem.* **2008**, *47* (6), 1727–1752.

(62) Cruz, A. J.; Kirgan, R.; Siam, K.; Heiland, P.; Rillema, D. P. Photochemical and Photophysical Properties of Ruthenium(II) Bis-Bipyridine Bis-Nitrile Complexes: Photolability. *Inorg. Chim. Acta* **2010**, *363* (11), 2496–2505.

(63) Juris, A.; Balzani, V.; Barigelletti, F.; Campagna, S.; Belser, P.; von Zelewsky, A. Ru(II) Polypyridine Complexes: Photophysics, Photochemistry, Electrochemistry, and Chemiluminescence. *Coord. Chem. Rev.* **1988**, *84*, 85–277.

(64) Ngo, K. T.; Lee, N. A.; Pinnace, S. D.; Szalda, D. J.; Weber, R. T.; Rochford, J. Probing the Noninnocent π-Bonding Influence of N-Carboxyamidoquinolate Ligands on the Light Harvesting and Redox Properties of Ruthenium Polypyridyl Complexes. *Inorg. Chem.* **2016**, *55* (5), 2460–2472.

(65) Cuéllar, E.; Méndez, A.; Pastor, L.; García-Herbosa, G.; Martín-Alvarez, J. M.; Miguel, D.; Villafañe, F. Manuscript in Preparation.

(66) Hameed, Y.; Gabidullin, B.; Richeson, D. Photocatalytic CO2 Reduction with Manganese Complexes Bearing a K2-PN Ligand: Breaking the α-Diimine Hold on Group 7 Catalysts and Switching Selectivity. *Inorg. Chem.* **2018**, *57* (21), 13092–13096.

(67) Kern, S.; van Eldik, R. Mechanistic Insight from Activation Parameters for the Reaction of a Ruthenium Hydride Complex with CO2 in Conventional Solvents and an Ionic Liquid. *Inorg. Chem.* **2012**, *51* (13), 7340–7345.

(68) Valeur, B. Molecular Fluorescence. In *digital Encyclopedia of Applied Physics*; Wiley-VCH Verlag GmbH & Co. KGaA: Weinheim, Germany, 2009; pp 477–531.

(69) Baba, H.; Goodman, L.; Valenti, P. C. Solvent Effects on the Fluorescence Spectra of Diazines. Dipole Moments in the (n,π*) Excited States 1. *J. Am. Chem. Soc.* **1966**, *88* (23), 5410–5415.

(70) Cheung, P. L.; Machan, C. W.; Malkhasian, A. Y. S.; Agarwal, J.; Kubiak, C. P. Photocatalytic Reduction of Carbon Dioxide to CO and HCO2H Using Fac-Mn(CN)(Bpy)(CO)3. *Inorg. Chem.* **2016**, *55* (6), 3192–3198.

(71) Rodrigues, R. R.; Boudreaux, C. M.; Papish, E. T.; Delcamp, J. H. Photocatalytic Reduction of CO 2 to CO and Formate: Do Reaction Conditions or Ruthenium Catalysts Control Product Selectivity? *ACS Appl. Energy Mater.* **2019**, *2* (1), 37–46.

(72) Fujita, E.; Creutz, C.; Sutin, N.; Szalda, D. J. Carbon Dioxide Activation by Cobalt(I) Macrocycles: Factors Affecting CO2 and CO Binding. *J. Am. Chem. Soc.* **1991**, *113* (1), 343–353.

(73) Gennaro, A.; Isse, A. A.; Vianello, E. Solubility and Electrochemical Determination of CO2 in Some Dipolar Aprotic Solvents. *J. Electroanal. Chem. Interfacial Electrochem.* **1990**, *289* (1–2), 203–215.

(74) Kamada, K.; Jung, J.; Wakabayashi, T.; Sekizawa, K.; Sato, S.; Morikawa, T.; Fukuzumi, S.; Saito, S. Photocatalytic CO2 Reduction Using a Robust Multifunctional Iridium Complex toward the Selective Formation of Formic Acid. *J. Am. Chem. Soc.* **2020**, *142* (23), 10261–10266.

(75) Dolomanoy, O. V.; Bourhis, L. J.; GIldea, R. J.; Howard, J. A. K.; Puschmann, H. No Title. *J. Appl. Crystallogr.* **2009**, *42*, 339–341.

(76) Sheldrick, G. M. Crystal Structure Refinement with SHELXL. *Acta Crystallogr. C.* **2015**, *71* (Md), 3–8.

(77) Sheldrick, G. M. A Short History of SHELX. *Acta Crystallogr. A.* **2007**, *64* (1), 112–122.

(78) Nardelli, M. Parst: A System of Fortran Routines for Calculating Molecular Structure Parameters from Results of Crystal Strucutre Analyses. *Comput. Chem.* **1983**, *7*, 95–98.

(79) Nardelli, M. PARST 95 – an Update to PARST: A System of Fortran Routines for Calculating Molecular Structure Parameters from the Results of Crystal Structure Analyses. *J. Appl. Crystallogr.* **1995**, *28* (5), 659–659.

(80) Jeffrey, G. A.; Lewis, L. Cooperative Aspects of Hydrogen Bonding in Carbohydrates. *Carbohydr. Res.* **1978**, *60* (1), 179–182.

(81) Taylor, R.; Kennard, O. Comparison of X-ray and Neutron Diffraction Results for the N-H ···O=C Hydrogen Bond. *Acta Crystallogr. B.* **1983**, *39* (1), 133–138.